Daily and 3-hourly variability in global fire emissions and consequences for atmospheric model predictions of carbon monoxide

M. Mu,[1] J. T. Randerson,[1] G. R. van der Werf,[2] L. Giglio,[3] P. Kasibhatla,[4] D. Morton,[5] G. J. Collatz,[5] R. S. DeFries,[6] E. J. Hyer,[7] E. M. Prins,[8] D. W. T. Griffith,[9] D. Wunch,[10] G. C. Toon,[11] V. Sherlock,[12] and P. O. Wennberg[10]

Received 12 May 2011; revised 23 September 2011; accepted 18 October 2011; published 24 December 2011.

[1] Attribution of the causes of atmospheric trace gas and aerosol variability often requires the use of high resolution time series of anthropogenic and natural emissions inventories. Here we developed an approach for representing synoptic- and diurnal-scale temporal variability in fire emissions for the Global Fire Emissions Database version 3 (GFED3). We disaggregated monthly GFED3 emissions during 2003–2009 to a daily time step using Moderate Resolution Imaging Spectroradiometer (MODIS)-derived measurements of active fires from Terra and Aqua satellites. In parallel, mean diurnal cycles were constructed from Geostationary Operational Environmental Satellite (GOES) Wildfire Automated Biomass Burning Algorithm (WF_ABBA) active fire observations. Daily variability in fires varied considerably across different biomes, with short but intense periods of daily emissions in boreal ecosystems and lower intensity (but more continuous) periods of burning in savannas. These patterns were consistent with earlier field and modeling work characterizing fire behavior dynamics in different ecosystems. On diurnal timescales, our analysis of the GOES WF_ABBA active fires indicated that fires in savannas, grasslands, and croplands occurred earlier in the day as compared to fires in nearby forests. Comparison with Total Carbon Column Observing Network (TCCON) and Measurements of Pollution in the Troposphere (MOPITT) column CO observations provided evidence that including daily variability in emissions moderately improved atmospheric model simulations, particularly during the fire season and near regions with high levels of biomass burning. The high temporal resolution estimates of fire emissions developed here may ultimately reduce uncertainties related to fire contributions to atmospheric trace gases and aerosols. Important future directions include reconciling top-down and bottom up estimates of fire radiative power and integrating burned area and active fire time series from multiple satellite sensors to improve daily emissions estimates.

Citation: Mu, M., et al. (2011), Daily and 3-hourly variability in global fire emissions and consequences for atmospheric model predictions of carbon monoxide, *J. Geophys. Res.*, *116*, D24303, doi:10.1029/2011JD016245.

1. Introduction

[2] In many parts of the world, fires exhibit considerable variability on timescales of hours to centuries [*Rothermel and Philpot*, 1973; *Johnson*, 1992; *Swetnam and Betancourt*, 1998; *Nepstad et al.*, 1999; *Gillett et al.*, 2004; *Mouillot and Field*, 2005; *Westerling et al.*, 2006; *Marlon et al.*, 2008]. Understanding the causes of this variability is important for assessing how fires respond to changes in climate and for

[1]Department of Earth System Science, University of California, Irvine, California, USA.
[2]Faculty of Earth and Life Sciences, VU University Amsterdam, Amsterdam, Netherlands.
[3]Department of Geography, University of Maryland, College Park, Maryland, USA.
[4]Nicholas School of the Environment and Earth Sciences, Duke University, Durham, North Carolina, USA.
[5]NASA Goddard Space Flight Center, Greenbelt, Maryland, USA.
[6]Department of Ecology, Evolution, and Environmental Biology, Columbia University, New York, New York, USA.
[7]Marine Meteorology Division, Naval Research Laboratory, Monterey, California, USA.
[8]Cooperative Institute for Meteorological Satellite Studies, University of Wisconsin-Madison, Madison, Wisconsin, USA.
[9]School of Chemistry, University of Wollongong, Wollongong, New South Wales, Australia.
[10]Divisions of Engineering and Applied Science and Geological and Planetary Science, California Institute of Technology, Pasadena, California, USA.
[11]Jet Propulsion Laboratory, California Institute of Technology, Pasadena, California, USA.
[12]National Institute of Water and Atmospheric Research, Ltd., Wellington, New Zealand.

0148-0227/11/2011JD016245

quantifying how fires influence atmospheric levels of greenhouse gases and aerosols [*Bowman et al.*, 2009]. Fire emissions have been shown, for example, to explain some of the interannual variability in atmospheric CH_4 [*Langenfelds et al.*, 2002; *Bousquet et al.*, 2006] and CO_2 [*Langenfelds et al.*, 2002; *van der Werf et al.*, 2004; *Randerson et al.*, 2005; *Nevison et al.*, 2008; *Prentice et al.*, 2011] and much of the seasonal and interannual variability in CO, particularly in tropical and southern hemisphere regions [*Bergamaschi et al.*, 2000; *Langenfelds et al.*, 2002; *Chen et al.*, 2010; *Kopacz et al.*, 2010]. Concurrent measurements of burned area have improved our understanding of various aspects of ecosystem function, including trajectories of post-fire net primary production [*Hicke et al.*, 2003; *Goetz et al.*, 2006] and surface energy exchange [*Jin and Roy*, 2005; *Lyons et al.*, 2008; *McMillan and Goulden*, 2008]. Motivation for studying higher frequency variability in burned area and emissions – over timescales shorter than one month – comes from another set of inter-related science questions. A key line of inquiry in these studies is the investigation of how diurnal and daily variability in emissions interact with atmospheric transport and chemistry to influence atmospheric composition, radiation, and air quality.

[3] Covariance of emissions with atmospheric transport and chemistry on daily and diurnal timescales can be substantial with important consequences for air quality. Fires in Southern California that occur during periods of Santa Ana winds, for example, have emissions that are often transported in a direction that is largely orthogonal to the mean atmospheric flow [*Moritz et al.*, 2010]. As a consequence, plumes from these fires often extend across urban areas with significant impacts on human health [*Delfino et al.*, 2009]. On diurnal timescales, interactions between the timing of emissions and the growth of the planetary boundary layer (PBL) influence plume dynamics, rates of vertical mixing of aerosols and trace gases, aerosol and trace gas lifetimes, and the lateral transport of these emissions within the free troposphere [*Wang et al.*, 2006; *Chen et al.*, 2009; *Reid et al.*, 2009; *Val Martin et al.*, 2010].

[4] Important aspects of atmospheric chemistry also respond on diurnal timescales, including processes that regulate the formation and destruction of NO, NO_2, and aerosols. Three spectrometers (Global Ozone Monitoring Experiment (GOME), Ozone Monitoring Instrument (OMI), and Scanning Imaging Absorption Spectrometer for Atmospheric Cartography (SCIAMACHY)) on three different satellites currently provide column measurements of NO_2, thus allowing for improved constraints on ozone chemistry and rates of nitrogen deposition in terrestrial and ocean ecosystems. Given the rapid photochemical oxidation of NO_2 during the day [*Boersma et al.*, 2008], use of column measurements in biomass burning regions to infer NO_x fluxes requires an understanding of the diurnal cycle of emissions. For example, *Boersma et al.* [2008] show that across southern Africa, South America, and other tropical regions with high fire emissions, column NO_2 mixing ratios detected by OMI with a 1330 LT overpass are more than 40% higher than similar measurements made by SCIAMACHY with a 1000 LT overpass. This temporal pattern is consistent with high levels of midday fire emissions [e.g., *Giglio*, 2007] that increase the column abundance of NO_2 between the two overpass times. The opposite diurnal pattern of column NO_2 is observed over fossil fuel source regions where emissions are more uniform during the day and thus NO_2 variations are more closely regulated by the diurnal cycle of loss processes that reach a maximum during midday.

[5] Aerosol models used for climate and air quality assessments [*Schulz et al.*, 2006; *Chin et al.*, 2009] have additional sensitivities to the time interval of fire emissions inventories. Emissions inventories with coarse time steps (i.e., 1 month) are often distributed within atmospheric models uniformly from day-to-day, increasing the probability that some emissions will be released during precipitation events or during meteorological conditions that are considerably different from those that occurred during the time of the fires. Higher resolution emissions inventories have the potential to reduce biases associated with these temporal and spatial mismatches [e.g., *Xian et al.*, 2009] and thus improve our understanding of direct and indirect climate forcing caused by biomass burning aerosols [*Jacobson*, 2001; *Ramanathan et al.*, 2001; *Kaufman et al.*, 2005; *Yu et al.*, 2006; *Flanner et al.*, 2007]. Compared to many other industrial aerosols sources, fire aerosol emissions are unique in that that they are closely coupled with synoptic to interannual variations in meteorology that influence fire behavior, including fuel moisture levels and fire spread rates, as well as dry and wet aerosol deposition rates. Although uncertainties associated with the timing of fire aerosol emissions are likely to be smaller than other factors, including uncertainty associated with condensation and coagulation of organic aerosols and bulk emissions [*Reid et al.*, 2005, 2009], improved daily emissions estimates are needed, nevertheless, to allow for realistic comparisons with satellite and surface aerosol optical depth observations.

[6] Here we describe an approach for representing synoptic and diurnal variability in fire emissions from the Global Fire Emissions Database version 3 (GFED3) monthly time series [*Giglio et al.*, 2010; *van der Werf et al.*, 2010]. Our approach builds on many past studies that have strengthened our understanding of daily and hourly controls of fire emissions and the impact of these emissions on atmospheric chemistry. *Heald et al.* [2003] created one of the first global fire emission inventories with a daily resolution, using Advanced Very High Resolution Radiometer (AVHRR) satellite observations to distribute fire emissions from a monthly climatology developed by *Duncan et al.* [2003]. Use of the polar-orbiting satellite observations at this time step required careful consideration of day-to-day variations in overpass coverage and cloudiness and the impacts of scan angle on the performance of the active fire detection algorithm. Although including diurnal variability in emissions across Asia did not significantly affect CO levels measured in remote aircraft transects over the Pacific, the impacts on surface CO were considerable near and within source regions. For the North American continent, *Wiedinmyer et al.* [2006] developed a daily 1 km fire emissions time series for 2002–2004 by combining active fire observations from MODIS with high spatial resolution information on vegetation cover (and thus fuel loads and emission factors) from the Global Land Cover (GLC2000) project [*Latifovic et al.*, 2004]. In northern boreal regions, both *Hyer et al.* [2007] and *Chen et al.* [2009] provide evidence that atmospheric simulations of CO are improved when monthly mean emissions time series are replaced by synoptic-scale (weekly) emissions.

[7] Over the past decade, the Fire Locating and Modeling of Burning Emissions (FLAMBE) modeling system also has been used operationally to forecast visibility and air quality at regional to global scales [*Reid et al.*, 2009]. This system integrates active fire products from Geostationary Operational Environmental Satellite (GOES) and polar orbiting (Terra and Aqua) sources with biome-specific fuel loads and emission factors to estimate emissions with an hourly time step. Using FLAMBE emissions with a meso-scale atmospheric model, *Wang et al.* [2006] show that biomass burning plumes from Central America are sometimes transported several hundreds of kilometers north by southerly winds, and model representation of these plumes is sensitive to diurnal variation in the smoke source. These plumes have significant effects on air quality and particulate matter concentrations across the south central and southeastern U.S. [*Wang et al.*, 2006] and may intensify severe weather events in the continental interior [*Wang et al.*, 2009].

[8] Diurnal variability in fire activity has been investigated in several remote sensing studies [e.g., *Langaas*, 1992; *Prins and Menzel*, 1992; *Eva and Lambin*, 1998; *Prins et al.*, 1998, 2001; *Giglio*, 2007; *Zhang and Kondragunta*, 2008; *Roberts et al.*, 2009]. These studies offer a perspective on fire variability that is broadly consistent with field observations and modeling of fire behavior on diurnal and synoptic timescales [*Show*, 1919; *Beall*, 1934; *Rothermel and Philpot*, 1973; *Beck and Trevitt*, 1989; *Linn et al.*, 2002; *McRae et al.*, 2005]. A quantitative understanding of diurnal cycle of fire dynamics is required for comparing estimates of fire radiative power from satellites with different overpass times and sensor characteristics [e.g., *Xu et al.*, 2010; *Roberts et al.*, 2011] and for modeling plume injection processes [*Freitas et al.*, 2007], in addition to the transport, chemistry and mixing processes described above. Several generalizations emerge from these studies of satellite observations of active fires. First, for most vegetation types, peak fire activity typically occurs during early and mid afternoon (between 1200 and 1600 LT) with fire activity at night often lower by an order of magnitude or more. The drop at night is consistent with lower sensible heat fluxes and wind speeds and higher levels of atmospheric humidity that limit rates of fuel consumption and fire spread rates [e.g., *McRae et al.*, 2005]. Second, diurnal patterns of fire activity vary with biome type, although the results are not always consistent among different studies. For example, croplands tend to have lower levels of burning at night compared to other fire types when analyzed using AVHRR [*Eva and Lambin*, 1998] and GOES [*Zhang and Kondragunta*, 2008] active fire products, but this pattern is not observed in some mixed crop and savanna regions by the Tropical Rain Measuring Mission (TRMM) Visible and InfraRed Scanner (VIRS) [*Giglio*, 2007]. Satellite observations of fires have not been used as widely to investigate relationships between diurnal patterns of fire activity and other factors such as spread rate, wind speed, humidity, and fire size. Increasing availability of enhanced fire products from multiple geostationary satellites over the next several years should improve our understanding of these biophysical controls as well as other socio-economic and cultural influences.

[9] Here we develop a global time series of fire emissions at a 0.5° × 0.5° spatial resolution that includes diurnal and synoptic-scale variability by combining information from MODIS and GOES WF_ABBA active fire products with a monthly emissions inventory derived from MODIS 500 m burned area [*Giglio et al.*, 2010; *van der Werf et al.*, 2010]. We then evaluated the impact of this variability on model estimates of atmospheric CO using Total Carbon Column Observing Network (TCCON) and Measurements of Pollution in the Troposphere (MOPITT) observations. In section 2 below (the methods) we describe key driver data sets, our methodology for developing our high frequency time series, and our modeling approach. In section 3 (the results) we compare our results with available atmospheric observations. In sections 4 and 5 (the discussion and conclusions), we evaluate important sources of uncertainty and identify directions for future investigation.

2. Methods

[10] We first describe the data sets and approaches we used to construct our daily and hourly emissions time series. We then provide information about the atmospheric model simulations used to evaluate how monthly, daily, and 3-hourly emissions time series influence our ability to estimate variability in atmospheric CO.

2.1. Global Fire Emissions Database Version 3

[11] GFED3 provides monthly estimates of burned area and carbon emissions for 1997–2009 at a 0.5° spatial resolution. Burned area for 2000–2009 was derived primarily from 500 m maps of surface reflectance from the Moderate Resolution Imaging Spectroradiometer (MODIS) on Terra and Aqua satellites using the direct broadcast algorithm from *Giglio et al.* [2009]. During times when surface reflectance observations were unavailable, a combination of local regression and regression tree approaches were used to estimate burned area from Terra MODIS active fire observations [*Giglio et al.*, 2010]. These same regression techniques were used to relate TRMM VIRS [*Giglio et al.*, 2003] and Along Track Scanning Radiometer (ATSR) [*Arino and Rosaz*, 1999] active fire observations to MODIS burned area, allowing for the extension of the GFED3 time series prior to the MODIS era (i.e., during 1997–2000). The monthly time step of GFED3 burned area was determined primarily by the need to temporally aggregate burned area and active fire observations to develop reliable regression models with TRMM and ATSR active fire products.

[12] Carbon emissions from GFED3 were obtained from a biogeochemical model that is driven by the burned area time series described above [*van der Werf et al.*, 2010]. Satellite observations provided important constraints on the spatial distribution of net primary production and fuel loads. Leaf senescence and allocation parameterizations were adjusted to match aboveground biomass observations in savanna and tropical forest ecosystems. Other significant improvements to the biogeochemical model in GFED3 included the use of newly available maps of peatlands in Indonesia to quantify soil organic matter levels, the use of subgrid-scale burned area in different vegetation types to estimate emission factors, and the calibration of a new fire-driven deforestation module using satellite observations of deforestation area. Uncertainty estimates for GFED3 carbon emissions were obtained using a Monte Carlo approach, with error distributions for burned area obtained from *Giglio et al.* [2010] and subjective error distributions assigned for fuel load and combustion

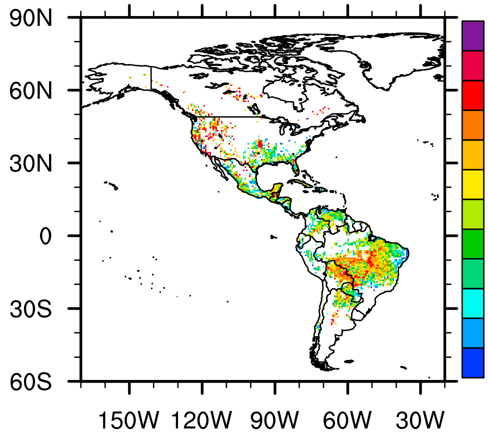

Figure 1. Correlation of daily active fire counts from GOES WF_ABBA and the sum of Aqua and Terra sensors during 2007–2009. Active fires from Terra were first adjusted using the regional factors shown in auxiliary material Table S1 to account for differences in satellite overpass times (relative to Aqua) that have consequences for sampling the diurnal cycle of fire activity. We only included in the analysis grid cells and years that had at least 10 GOES WF_ABBA active fire observations and 10 Aqua or Terra observations each year. The GOES program spatial domain encompasses North, Central, and South America: the GOES 11 (West) and 12 (East) satellites were positioned during this time period over the equator at 135°W and 75°W.

completeness components of the model [*van der Werf et al.*, 2010].

2.2. MODIS and GOES Active Fires

[13] We used MODIS active fire observations to distribute monthly emissions estimates from GFED3 to a daily temporal resolution in 0.5° × 0.5° grid cells. For this, we used collection 5 of the Global Monthly Fire Location Product (MCD14ML) [*Giglio et al.*, 2006] that includes separate lists of active fires for Aqua and Terra. This product contains the individual locations and times of active fires from day and night MODIS overpasses at a 1 km spatial resolution. The MODIS resolution varies from 1 km at nadir to 2.0 km by 4.8 km at a scan angle of 55°. We screened and removed persistent active fire locations associated with volcanoes, gas flaring, and other non-fire sources using a static hot spot database [*Giglio et al.*, 2006]. In our analysis, we included all of the MODIS active fire detections – we did not screen the observations using confidence intervals. In contrast to some of the temporally and spatially aggregated MODIS active fire count products, MCD14ML does not include any corrections for variable cloud cover or gaps in satellite coverage. As described below in section 2.3, we adjusted our approach to take into account latitudinal changes in Aqua and Terra satellite coverage based on comparisons with the GOES active fire time series in the Western Hemisphere.

[14] We used GOES WF_ABBA active fire data [*Prins et al.*, 1998; *Reid et al.*, 2009] to construct climatological mean diurnal cycles of fire activity. We specifically used GOES-11 (west) and GOES-12 (east) observations during 2007–2009 with version 6.0 of the WF_ABBA algorithm. This time period includes seasonal and interannual variations in burning due to climatic and socio-economic forcing mechanisms. We used these observations to construct a single mean diurnal cycle for each of several different vegetation types within different continental-scale regions as described below. In future work, observations from an updated version of the WF_ABBA (version 6.5) may allow for more detailed characterizations of diurnal cycles during different periods within the fire season or as a function of environmental conditions.

[15] We only used the full hemispheric scans that occurred every three hours from each satellite to build our mean diurnal cycles because these scans were less likely to be affected by rescheduling issues associated with tracking hurricanes and other weather phenomena. Our analysis does not account for block-out zones due to solar contamination near local noon and cloud obscuration. For the 3-hourly data set used in this study, the solar contamination block-out zone primarily impacts local noon observation of fires in Florida, several gulf coast states, and the Yucatan Peninsula in the late spring and early summer. It also inhibits fire detection near local noon in northeastern Brazil in the spring and fall. We chose these two satellites and time period because of the higher saturation temperatures of the 3.9 μm channel on these radiometers compared to earlier GOES-10 and GOES-9 instruments. We only used fire pixels for which the retrieval algorithm had higher levels of certainty (classes 0–3), where 0 represented the highest quality in which sub-pixel estimates of instantaneous fire size and temperature were retrieved from the WF_ABBA, 1 represented saturated fire pixels, 2 represented cloud contaminated fire pixels, and 3 represented high probability fire pixels. The spatial resolution of the GOES observations varies, from approximately 4 km at nadir to ~8 km at 60° latitude [*Reid et al.*, 2009].

2.3. Approach for Estimating Daily Fire Emissions Fractions

[16] Within each 0.5° grid cell for which GFED3 monthly emissions were available, we estimated the daily fraction of emissions using the sum of Terra and Aqua active fires. Prior to combining the Terra and Aqua time series, the Terra fire counts were multiplied by a regionally specific factor that was computed as the ratio of mean annual daily Aqua active fires to mean annual daily Terra active fires (auxiliary material Table S1).[1] This adjustment represented an attempt to normalize for regional differences in the diurnal cycle of fire activity as sampled by Terra (10:30 am/10:30 pm LT) as compared to Aqua (1:30 pm/1:30 am LT). For most regions, these factors were greater than 1 which meant that by applying the adjustment factor Terra active fires were amplified – giving this time series proportionally greater weight because of the lower probability of observing fires in mid-morning as compared to early afternoon [e.g., *Giglio*, 2007]. Agreement between this adjusted sum and GOES WF_ABBA active fires was relatively high in boreal forests across Alaska and Canada, in western forests in the U.S., and in dry tropical forests in southern Mexico (Figure 1). Correlations were also high in South America across Bolivia and in the Brazilian states of Rondonia, Mato Grosso, and

[1]Auxiliary materials are available in the HTML. doi:10.1029/2011JD016245.

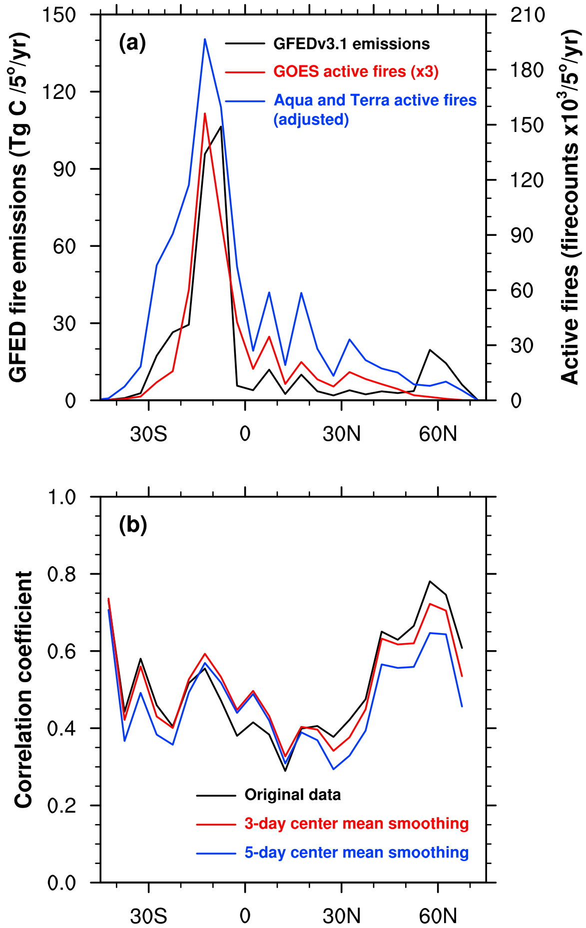

Figure 2. (a) Zonal sums of GFED3 fire emissions for 5° latitude bands (Tg C/yr) and annual mean active fire counts from GOES and the sum of Aqua and Terra MODIS during 2007–2009 in the Western Hemisphere. (b) The mean correlation coefficients between daily GOES WF_ABBA active fires and the sum of Aqua and Terra active fires (with overpass adjustments to Terra) for three different levels of smoothing: no smoothing, a 3-day centered mean smoothing filter, and a 5-day centered mean smoothing filter. The mean correlation coefficients shown here are the mean of all the individual grid cell correlation coefficients within each latitude band. In both panels, active fires from Terra were first adjusted using the regional factors shown in auxiliary material Table S1 to normalize for differences in satellite overpass times (relative to Aqua).

Tocantins. The relationship between MODIS and GOES was weaker in the easternmost states of Brazil and across the southeastern U.S., possibly as a result of smaller and more sporadic agricultural or forest management fires that have lower detection probabilities for both sensors. Furthermore portions of these regions are impacted by the GOES WF_ABBA solar contamination block-out zones in spring and fall.

[17] As a consequence of satellite orbital geometry, coverage by Aqua and Terra increased toward the poles, reducing the size of spatial gaps between successive overpasses. In the tropics, these gaps created an artificial spikiness in the distribution of active fires that had the potential to bias estimates of daily emissions [e.g., *Al-Saadi et al.*, 2008] (auxiliary material Figure S1). By smoothing the MODIS active fire time series in each 0.5° grid cell using 3-day and 5-day center mean filters, correlation between the MODIS time series and GOES WF_ABBA active fires increased in the tropics, particularly between 15°N and 15°S (Figure 2). In contrast, in mid and high latitudes where there were fewer gaps in coverage by MODIS (and there was less evidence for spikiness as shown in auxiliary material Figure S2), smoothing degraded the correlation with GOES.

[18] To account for the latitudinal differences in MODIS coverage, we generated our daily fraction of emissions using a 3-day center mean smoothing filter equator-ward of 25°N and 25°S and no smoothing filter pole-ward of these latitudes. This approach is similar to past work aggregating Aqua and Terra active fires in two day intervals in equatorial regions to avoid satellite overpass gaps for near real time biomass burning emissions estimates [*Al-Saadi et al.*, 2008; *Pierce et al.*, 2009]. Thus our daily emissions fractions represented a true 1-day time step in the extra-tropics, and ~3 day time step in the tropics and subtropics. We opted to accept this lower resolution for the tropics and subtropics of the Western Hemisphere where hourly GOES observations were available to allow for a consistent treatment across the tropics as a whole by MODIS. As the availability of active fire observations from other geostationary satellites increases in the future [e.g., *Reid et al.*, 2009], we expect refinements to this approach and significant reductions in uncertainties associated with daily emissions estimates in tropical Africa and Asia.

[19] Following the approach described above, we generated a time series of daily fire fractions for each month in the GFED3 time series during 2003–2009, each with a variable number of days corresponding to the length of each month (and taking into account leap years).

2.4. Approach for Estimating 3-Hourly Fire Emissions Fractions

[20] We constructed climatological mean diurnal cycles of fire activity from GOES WF_ABBA active fire detections, as a function of vegetation type and region using all available GOES satellite observations from full hemisphere scans during 2007–2009. We then created a diurnal cycle of eight 3-hourly fractions of emissions for each 0.5° grid cell and month, using sub-grid scale information on burned area in different vegetation types from *Giglio et al.* [2010] to weight the contribution of different diurnal cycles to the grid cell mean during each month. Thus the shape of the diurnal cycle in a given grid cell varied from one month to the next, depending on the distribution of burned area in different vegetation types.

[21] To construct mean diurnal cycles of fire activity from measurements spanning multiple time zones, we used the following method. GOES WF_ABBA active fire detections had a Greenwich Mean Time (GMT/UTC) time stamp associated with them. We converted these UTC time stamps to local solar time (LST) at each grid cell by using the following equation: LST = UTC + longitude/15.

[22] Mean diurnal cycles of GOES WF-ABBA active fires for different regions and vegetation types in the Western Hemisphere, normalized to the same daily sum, are shown in Figure 3. The corresponding absolute levels of

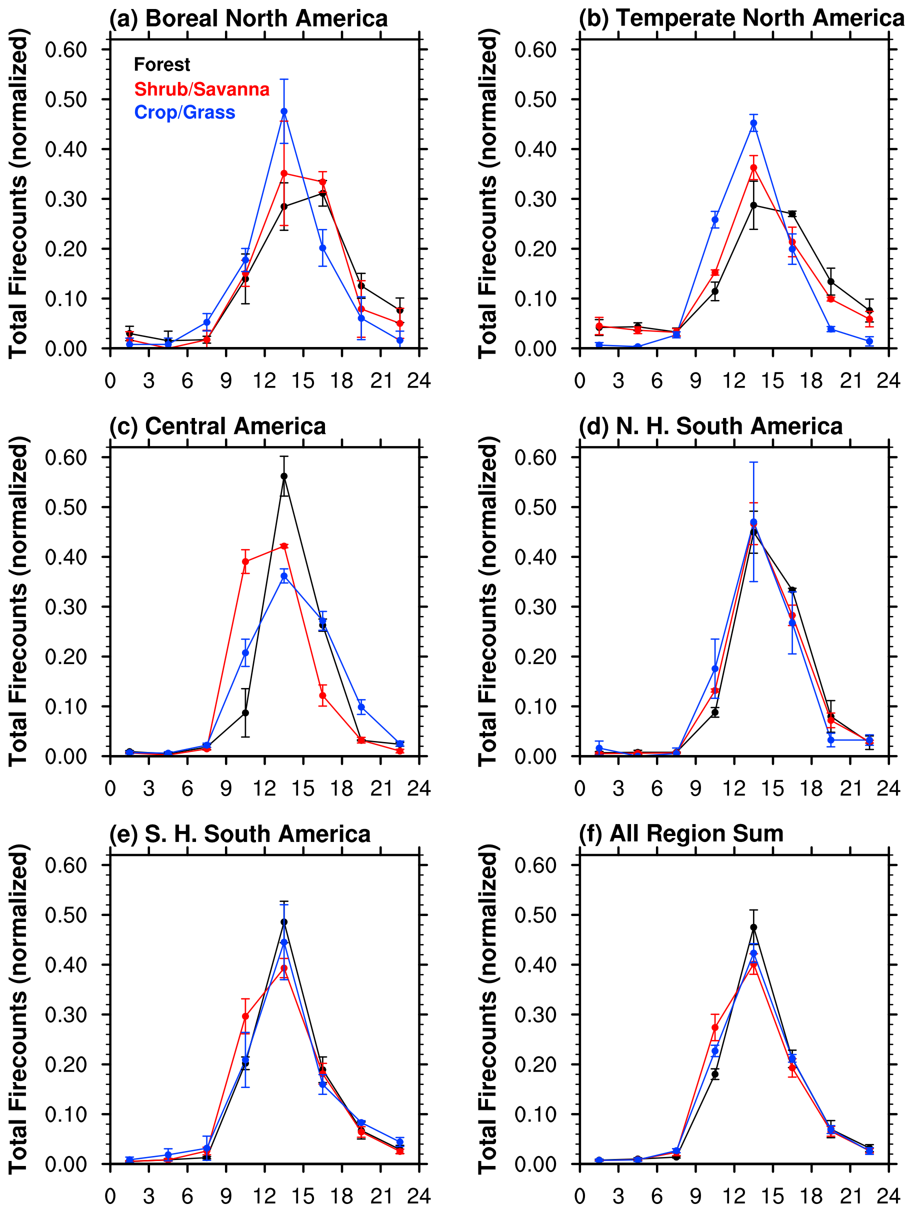

Figure 3. Diurnal cycles of fires constructed using GOES WF_ABBA active fire counts from 2007 to 2009. The different diurnal cycles were constructed only using grid cells at a 0.05° × 0.05° resolution each within region that had 80% or more coverage by each vegetation type. The fire counts have been normalized so that the sum for each individual vegetation type equaled 1 over a 24-h period. Each individual time step is 3 h. All valid observations during 2007–2009 were averaged together to construct the annual mean diurnal cycle shown here for each vegetation type. Error bars were calculated as the standard deviation of normalized annual mean fractions for each year.

active fires observed for each region and vegetation type are shown in auxiliary material Figure S3. These mean diurnal cycles were constructed only from 0.05° areas within each region that had greater than 80% coverage of one of the three aggregated vegetation types: forests, shrublands and savannas, or croplands and grasslands. We used the Terra MODIS collection 4 MOD12C1 land cover product [*Friedl et al.*, 2002] to identify these areas, and derived our aggregated vegetation types from the International Geosphere Biosphere Program (IGBP) classification within this product. Specifically, we included the IGBP classes of evergreen needleleaf forest, evergreen broadleaf forest, deciduous needleleaf forest, deciduous broadleaf forest, and mixed forest in our aggregated forest class, closed and open shrubland, woody savannas, and savannas in our aggregated shrubland and savanna class, and grasslands, croplands, cropland/natural vegetation mosaic, and barren or sparsely vegetated areas in our grassland and cropland class. Our logic was to broadly separate vegetation types into three classes as a function of high, medium and low fuel densities. The distribution of burned area in these three aggregated vegetation types is summarized in auxiliary material Figures S4 and S5 and

Table 1. Fraction of Burned Area in Different Aggregated Vegetation Classes During 2003–2009

Region[a]	Forests	Shrublands and Savannas	Croplands and Grasslands
BONA[b]	0.558	0.400	0.042
TENA	0.239	0.311	0.450
CEAM	0.327	0.360	0.312
NHSA	0.109	0.618	0.272
SHSA	0.199	0.643	0.158
EURO	0.177	0.323	0.500
MIDE	0.016	0.273	0.710
NHAF	0.053	0.800	0.147
SHAF	0.075	0.875	0.049
BOAS	0.295	0.394	0.311
CEAS	0.029	0.062	0.909
SEAS	0.225	0.356	0.419
EQAS	0.783	0.145	0.072
AUST	0.027	0.897	0.076

[a]Abbreviations for the different regions are as follows: BONA, boreal North America; TENA, temperate North America; CEAM, Mexico and Central America; NHSA, northern hemisphere South America; SHSA, southern hemisphere South America; EURO, Europe; MIDE, the Middle East; NHAF, northern hemisphere Africa; SHAF, southern hemisphere Africa; BOAS, boreal Asia; CEAS, central Asia; SEAS, Southeast Asia; EQAS, equatorial Asia; AUST, Australia and Oceania. A spatial map of the distribution of these regions is given in auxiliary material Figure S6.

[b]The MODIS land cover product classified open taiga forests in boreal North America and boreal Asia as open shrubland, and in some instances, savanna. These ecosystems are very different from subtropical savanna and shrublands, with one notable difference being the presence of large stores of carbon in organic soils that are vulnerable to combustion.

Table 1 for different continental-scale regions shown in auxiliary material Figure S6.

[23] To develop our global product, we applied the normalized diurnal fractions for the 3 different vegetation classes from GOES (Figure 3) to regions with roughly similar biogeography. For example, we used normalized diurnal fractions from boreal North America in boreal Asia. The complete mapping is provided in Table 2. This mapping approach may be further refined when geostationary active fire observations from other platforms become publicly available for ecosystems in Africa and Asia [e.g., *Reid et al.*, 2009].

2.5. Atmospheric Model Simulations

[24] To simulate atmospheric CO we used the GEOS-Chem global three-dimensional model of tropospheric chemistry [*Bey et al.*, 2001] which was driven by assimilated meteorological observations from the Goddard Earth Observation System (GEOS) of the NASA Global Modeling and Assimilation Office (GMAO). We used version 8-01-02 of the model (http://acmg.seas.harvard.edu/geos/) driven by GEOS-5 reanalysis [*Rienecker et al.*, 2008] that had 72 vertical layers and was averaged to a 2° × 2.5° horizontal resolution. The new GEOS-5 reanalysis used a modified relaxed Arakawa-Schubert convection scheme [*Ott et al.*, 2009] that led to improvements in the distribution of precipitation and atmospheric circulation across the tropics as compared to GEOS-4.

[25] Our model simulations spanned the 2004 to 2009 period, after a spin up period of one year. For the spin-up, we used 2004 meteorology (the first available year of the GEOS-5 reanalysis that was modified to drive GEOS-Chem) and monthly, daily or 3-hourly fire emissions from 2003. In these simulations, we carried three separate tracers for monthly GFED3 CO emissions and the daily and 3-hourly emissions time series we developed here (the latter two tracers are described above in sections 2.3 and 2.4). We chose to inject fire emissions into the surface layer of the atmospheric model because several recent remote sensing studies indicate that most fire plumes remain within the planetary boundary layer [*Val Martin et al.*, 2010; *Tosca et al.*, 2011]. We saved 3-hourly distributions of CO mixing ratio from the model for all three tracer simulations, and sampled the three-dimensional distribution of CO mixing ratio at the time and location of the MOPITT satellite measurements and TCCON stations as described below.

[26] In addition to the fire emissions tracers described above, we also included CO emissions from anthropogenic, biofuel and biogenic emissions in the GEOS-Chem model simulations (auxiliary material Table S2). The sources of fossil fuel emissions were from *Streets et al.* [2006]. Biofuel emissions were from the inventory of *Yevich and Logan* [2003]. Isoprene and monoterpene CO sources were prescribed using a multiyear annual cycle mean (2004–2009) generated from the Model of Emissions of Gases and Aerosols from Nature driven by GEOS-5 meteorology (MEGAN) [*Guenther et al.*, 2006]. Methanol emissions were scaled based on results from MEGAN and acetone emissions were prescribed following *Jacob et al.* [2002]. All CO simulations used the same monthly 3-D OH concentration fields archived from a GEOS-Chem full-chemistry simulation [*Fiore et al.*, 2003].

2.6. Atmospheric Observations

[27] We compared our GEOS-Chem model simulations with TCCON CO observations from six sites: Park Falls, Lamont, JPL, Darwin, Wollongong, and Lauder. We selected these six sites based on the length of the available time series (longer than one year during the period of 2004–2009) and the requirement that fire-emitted CO visibly contribute to some of the observed variability of column CO at the different stations based on our monthly mean simulations with GEOS-Chem. This effectively excluded stations near urban

Table 2. Mapping of Regions in the Western Hemisphere to Other Parts of the World for the Purpose of Constructing Diurnal Cycles of Fire Emissions

Western Hemisphere (GOES Observations Available)	Rest of World (Diurnal Cycles Constructed From GOES Observations in Corresponding Western Hemisphere Regions)
Boreal North America (BONA)	Boreal Asia (BOAS)
Temperate North America (TENA)	Europe (EURO) and Central Asia (CEAS)
Central America and Mexico (CEAM)	Middle East (MIDE)
Northern Hemisphere South America (NHSA)	Northern Hemisphere Africa (NHAF)
Southern Hemisphere South America (SHSA)	Southeast Asia (SEAS), Equatorial Asia (EQAS), Southern Hemisphere Africa (SHAF), and Australia and Oceania (AUST)

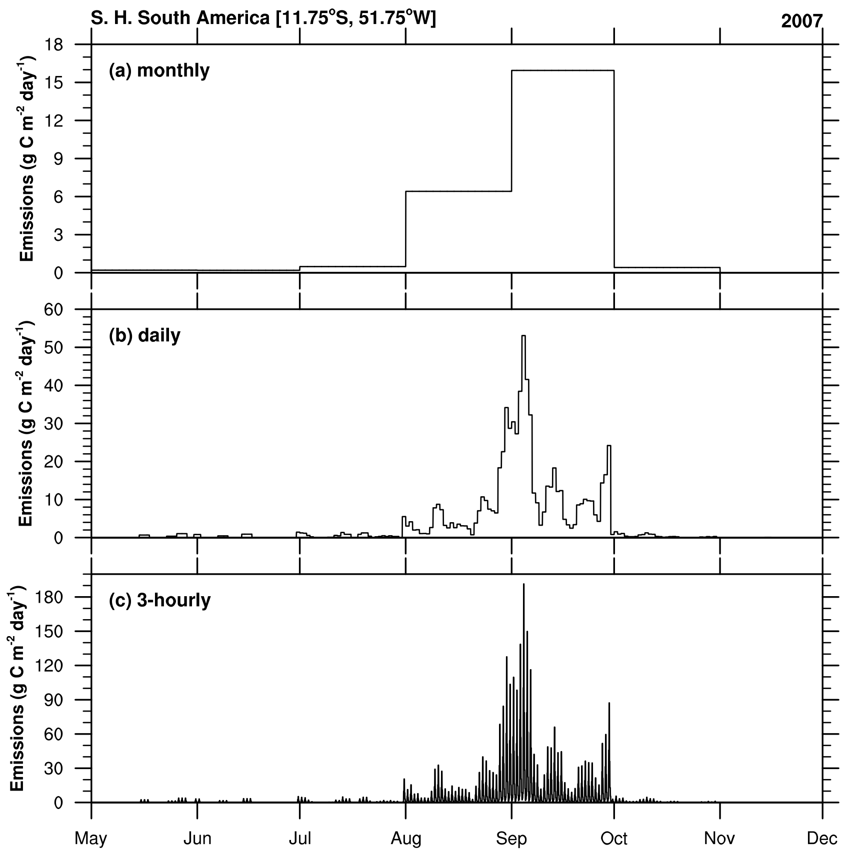

Figure 4. (a) Monthly GFED3 emissions averaged over a single 0.5 grid cell in northern South America (11.75°S, 51.75°W) during 2007. This grid cell was located in the northeastern corner of the Brazilian state of Mato Grosso. (b) Daily emissions and (c) 3-hourly emissions for the same grid cell derived using the approach described in the text. Note the different vertical scales.

areas with the exception of JPL. We used the beta version of the public TCCON data archive (http://tccon.ipac.caltech.edu/). TCCON is a global network of ground-based and sun-viewing Fourier Transform Infrared (FTIR) spectrometers designed to measure column abundances of CO, CO_2, CH_4, N_2O and other molecules that absorb in the near infrared [*Wunch et al.*, 2011]. Within the network, stringent requirements on the instrumentation, data processing and calibration have improved the accuracy and precision of the measurements [*Wunch et al.*, 2011]. Past work with TCCON observations has led to an identification of biases in vertical mixing in atmospheric models [*Yang et al.*, 2007], improved estimates of CH_4 emissions from the city of Los Angeles [*Wunch et al.*, 2009], reduced uncertainties associated with emission factors from savanna fires [*Paton-Walsh et al.*, 2010] and new diagnostics of the magnitude of seasonal carbon exchange in temperate and boreal ecosystems [*Keppel-Aleks et al.*, 2010]. TCCON retrievals of CO have been calibrated against in situ aircraft profiles at three sites: Lamont, Lauder, and Park Falls, and the calibration coefficient determined from these three sites is applied to all TCCON CO data [*Wunch et al.*, 2010]. Based on these comparisons, the estimated TCCON CO column dry air molar fractions have an accuracy of ±4 ppbv. Averaging kernels for CO peak in the upper troposphere/lower stratosphere such that the sensitivity to CO at 100 hPa is more than double that at the surface [*Wunch et al.*, 2010]. Diurnal and synoptic variability in TCCON CO total column measurements due to fires in the vicinity of a given site therefore may be damped because associated variations in CO are expected to occur primarily at the surface and in the lower troposphere.

[28] TCCON spectrometers require a direct view of the sun to measure atmospheric absorption. Under clear-sky conditions, an interferogram is typically recorded in less than 2 min. The exact time depends on how quickly the scanning mirror is moving and the spectral resolution of the spectrometer. When clouds are present, interferograms unaffected by cloud will be recorded less frequently, and integrating times can exceed 10 min. To compare the model with the observations, we first averaged all the column CO observations together within each 3-h interval of model output. We also computed the mean solar zenith angle (SZA) of the observations within each interval, and used this mean SZA with a look up table of averaging kernels (e.g., auxiliary material Figure S7) to estimate the column CO from GEOS-Chem.

[29] We also compared our simulations with the MOPITT version 4 daily level 3 CO product [*Deeter et al.*, 2003; *Emmons et al.*, 2004]. Improvements in the MOPITT version 4 product included a finer vertical resolution, a floating surface level, a lognormal distribution for CO volume mixing ratio (VMR) variability, and CO a priori that

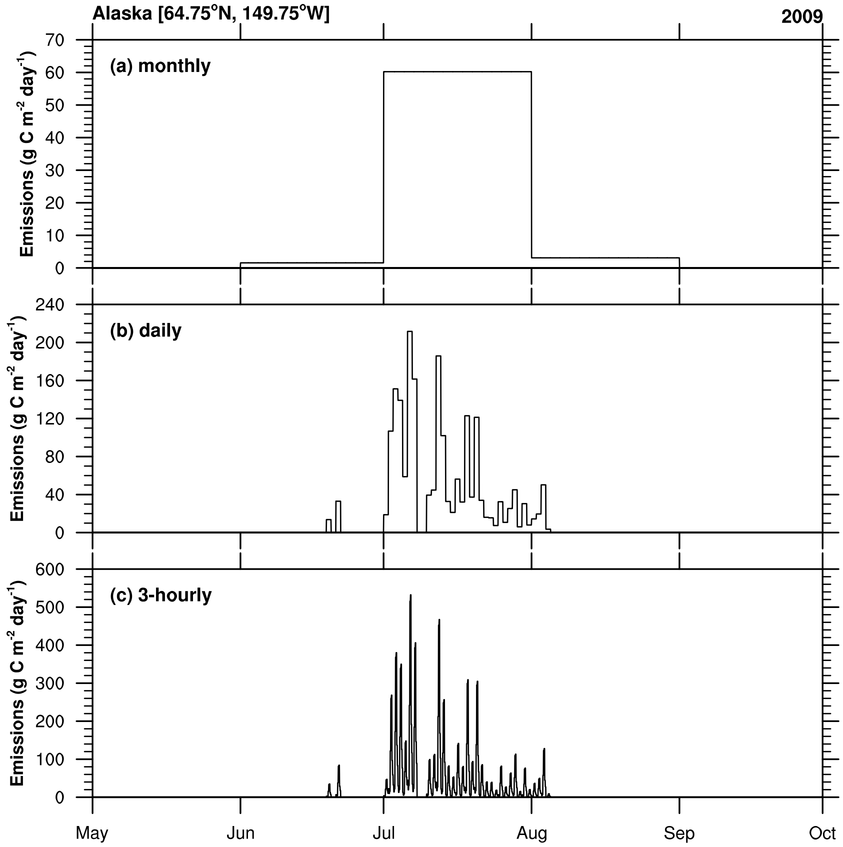

Figure 5. Same as Figure 4 but for a 0.5° grid cell in interior Alaska (64.75°N, 149.75°W) during 2009.

varied spatially and temporally [*Deeter*, 2009]. To compare with our model simulations, we only used daytime MOPITT observations, sampling the model during the 10:30 am MOPITT overpass time. We only included level 3 observations in our analysis for which the degree of freedom was greater than 0.98. We used MOPITT averaging kernels and a priori to construct the model CO column following the instructions for MOPITT version 4 data set [*Deeter*, 2009]. To compare MOPITT with the TCCON column CO we first smoothed the MOPITT retrievals using the TCCON averaging kernel following the approach described by *Luo et al.* [2007] and *Rodgers and Connor* [2003]. We did not compare our model simulations with surface CO observations because long-term time series of daily measurements were not available for many sites.

3. Results

3.1. Daily and 3-Hourly Fire Emissions for Individual Grid Cells

[30] Figures 4 and 5 show examples of the original monthly GFED3 emissions, these monthly emissions distributed to a daily time step derived from the sum of Aqua and Terra active fires (section 2.3), and 3-hourly emissions derived by adding diurnal information from GOES active fires (section 2.4) for 0.5° grid cells from South America and Alaska. For South America we show a representative grid cell from the northeastern corner of the Brazilian state of Mato Grosso during 2007, an area that has undergone extensive deforestation over the last decade (Figure 4). In this region, fires are often used to clear forests for mechanized agriculture and pasture [*Morton et al.*, 2008]. They also are used, to a lesser degree, to maintain forage quality in existing pastures, although most of the emissions are associated with forest clearing [*van der Werf et al.*, 2009]. For this cell, much of the burning occurred during a single two-week period in late August and early September.

[31] For Alaska we show a grid cell that was partly burned during the summer of 2009 as a part of the Minto Flats South fire (Figure 5). Measurements from within fire perimeters that burned during 2004 in Alaska yielded a mean fire combustion rate of 3300 g C per m^2 of burned area with a range of 1500–4600 g C per m^2 of burned area [*Boby et al.*, 2010]. Mean fuel consumption levels from GFED3 for this 2009 fire were somewhat higher but within the reported range: 3607 g C per m^2 of burned area for the grid cell shown in the figure. The active fire observations indicated that almost all of the burning in this grid cell occurred during July and the first week of August, with the most intense period of burning occurring during the first week of July. For both grid cells, the distribution of burning within the growing season was modified considerably by using active fires to distribute fire emissions on a daily basis.

3.2. Global Patterns of Daily Fires

[32] Global patterns of daily fires have the potential to provide new information about fire type and ecosystems processes. Key metrics of daily fire activity varied considerably

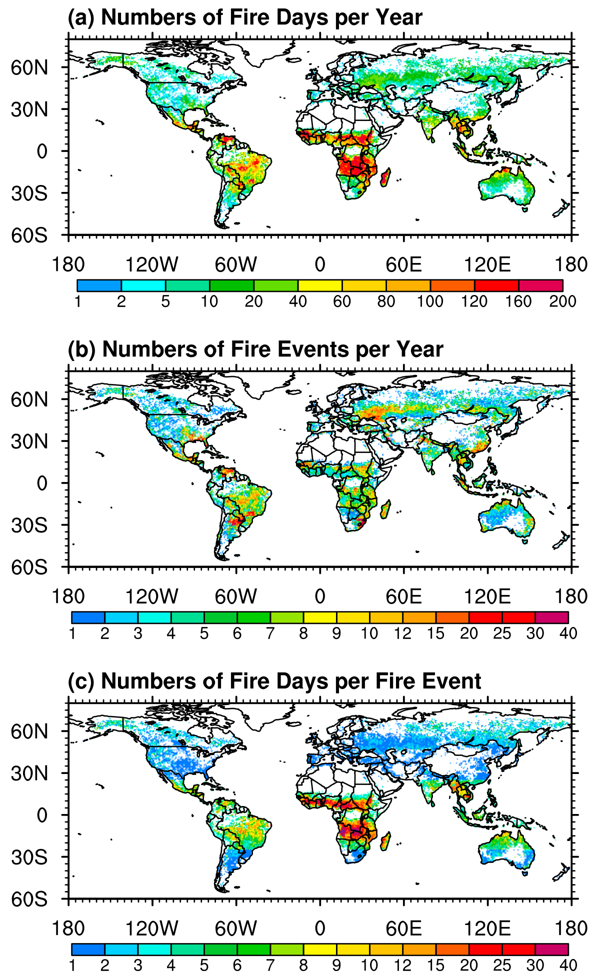

Figure 6. Global annual mean distribution of (a) the number of fire days per year, (b) the number of fire events per year, and (c) the number of fire days per fire event. These maps were generated using the daily fire fraction time series described in the main text (section 2.4) during 2003–2009. Figure 6c was constructed by dividing Figure 6a by Figure 6b. A fire event was defined as a single continuous period for which the daily fire fraction time series was nonzero. This meant that at least one Aqua or Terra active fire observation existed for that day in the extra-tropics (north of 25°N and south of 25°S), and the same for the tropics, but with a 3-day center-mean smoothing applied to compensate for gaps in satellite coverage. In the construction of Figures 6a and 6b, if a grid cell did not have any fires in a given year, this year was excluded from the multiyear mean shown in the panel.

among different biomes (Figure 6). The mean number of fire days each year, for example, ranged between 5 and 20 in many boreal ecosystems to over 100 in many savanna regions of South America and Africa (Figure 6a). The number of fire events each year, defined as the number of continuous periods of fire activity, also was higher in savannas (4–25 events) compared to boreal forests (2–6 events) but the relative difference between these two biomes was smaller than for the number of fire days (Figure 6b). As a result, the number of fire days per event was considerably higher in savannas compared to boreal forests (Figure 6c).

[33] It is important to note that these patterns are scale dependent (and were generated here at the 0.5° spatial resolution of GFED3). They also were influenced by the 3-day center mean smoothing we applied to active fires in tropical regions. Nevertheless, the relative spatial distributions suggested several interesting features of global fire behavior. The small number of days per fire event in boreal regions, for example, provided evidence that these fires were short-lived but intense given the relatively high levels of fuel consumption typical for this biome (Table 3). In contrast, the large number of fire days and large number of days per fire event in savanna regions indicated a more continuous pattern of burning over the fire season. Additional information on fire sizes derived from 500 m burned area data would be required to assess whether this pattern in savannas was driven by multiple independent small fires (of short duration) or a smaller number of large fires that moved slowly across the landscape.

[34] Agricultural fires also had a unique signature as quantified using these metrics. Across the Southeastern U.S., central Asia, and southern China, fires in these regions were characterized by a high number of individual fire events each year (Figure 6b) and a very low duration for each event (1–2 days) (Figure 6c).

[35] Daily rates of fire emissions, derived from mean annual emissions from *van der Werf et al.* [2010] and from the number of fire days per year described above, were considerably higher in boreal forest biomes of North America and Siberia than in other regions (Figure 7). The daily rate of fire emissions per unit of burned area, a metric which is related to both fuel consumption and rates of fire spread, was more than 70 times higher in boreal forests ecosystem of North America than in African savannas (Table 3).

3.3. Hemispheric Patterns of 3-Hourly Fires

[36] Most fire activity occurred in the middle of the day and this was especially the case for Central and South America where 35%–56% of all fires in different biome types occurred during the 3-h interval between 12:00–15:00 LT. In contrast, the least amount of fire activity in all regions and biome types occurred after midnight, between 0:00–09:00 LT, with the sum during this 9 h interval never exceeding 13% of the 24-h total (Figure 3). In tropical biomes, these diurnal patterns are in general agreement with results from earlier satellite remote sensing studies [e.g., *Langaas*, 1992; *Prins et al.*, 2001; *Giglio*, 2007; *Roberts et al.*, 2009].

[37] The smallest diurnal amplitudes of fire activity occurred in forest and shrub biomes of boreal and temperate North America. Fires in these biomes had considerably higher levels of burning in late afternoon and evening relative to fires in other regions and ecosystems (Figure 3). This shift in the diurnal cycle is consistent with longer duration fires and thus stronger controls on fire spread rates from synoptic-scale meteorological events that persist for multiple days [e.g., *French et al.*, 2011] and with fire behavior studies in North American forests that indicate optimal weather conditions for fire spread peak in mid afternoon between 2 and 4 P.M. LT [*Beall*, 1934; *Beck and Trevitt*, 1989]. For temperate North America, the reduced diurnal amplitude and higher levels of fire activity during evening observed for forest fires relative to cropland fires is consistent with earlier analyses of GOES observations using a different land cover classification

Table 3. Summaries for Mean Annual Burned Area (Mha/yr), Mean Annual Fire Emissions (Tg C/yr), Fuel Consumption (g C per m^2 of Burned Area), Number of Fire Days per Year, Daily Rate of Burned Area (% of Annual Burned Area/Day), and Daily Rate of Fuel Consumption (g C/m^2 of Burned Area/Day) Averaged During 2003–2009

Region	Mean Annual Burned Area (Mha/yr)	Mean Annual Emissions (Tg C/yr)	Fuel Consumption (g C per m^2 of Burned Area)	Number of Fire Days[a] (d/yr)	% of Annual Burned Area per Day	Daily Rates of Fuel Consumption (g C per m^2 of Burned Area per Day)
BONA	2.3	64	2764	7.2	13.9	383
TENA	1.6	10	621	10.5	9.5	59
CEAM	1.3	18	1442	54.5	1.8	26
NHSA	2.3	22	966	75.8	1.3	13
SHSA	17.7	299	1692	51.6	1.9	33
EURO	0.6	4	660	9.4	10.6	70
MIDE	0.9	2	206	12.6	7.9	16
NHAF	120.0	447	372	86.1	1.2	4
SHAF	126.8	570	449	95.1	1.1	5
BOAS	6.2	110	1762	10.2	9.8	173
CEAS	13.6	34	249	15.9	6.3	16
SEAS	7.6	106	1383	43.7	2.3	32
EQAS	1.1	116	10677	42.5	2.4	251
AUST	39.8	121	305	28.4	3.5	11
Global sum or mean:	341.7	1922	1682	38.8	5.3	78

[a]The mean number of fire days refers to the number of separate days that had active fire observations in 0.5° grid cells that had some burned area during the calendar year. Only grid cells within each year for which burned area was detected were used to construct the biome-level mean for each year.

[*Zhang and Kondragunta*, 2008]. Forest and shrubland biomes in boreal North America had similar diurnal patterns of fire activity. This was consistent with the MODIS-derived land cover classification we used that assigned areas with lower levels of evergreen tree cover (e.g., taiga) to shrub and savanna classes.

[38] In Central and South America, small differences in phase were visible between the timing of forest fires relative to shrubland/savanna and cropland/grassland fires (Figure 3). Fires in the latter two biome classes started increasing earlier in the morning and often tapered off at earlier times in the afternoon. One possible mechanism explaining this pattern is that crop, grass and shrub fuels dry out faster than forest fuels, enabling land managers to start the ignition process earlier in the day [*Giglio*, 2007]. This explanation is consistent with observations that show intact tropical forest canopies have higher levels of surface humidity that are known to inhibit fire activity [*Nepstad et al.*, 2004]. Higher levels of fuels in forests also may enable longer periods of burning that persist into late afternoon and evening. It is important to note in the context of interpreting these results that other remote sensing studies of tropical fire show diverging diurnal patterns as a function of vegetation type. For example, in an analysis of Tropical Rainfall Measuring Mission observations, *Giglio* [2007] found that fires in tropical forests peaked earlier in the day than fires occurring in ecosystems with lower levels

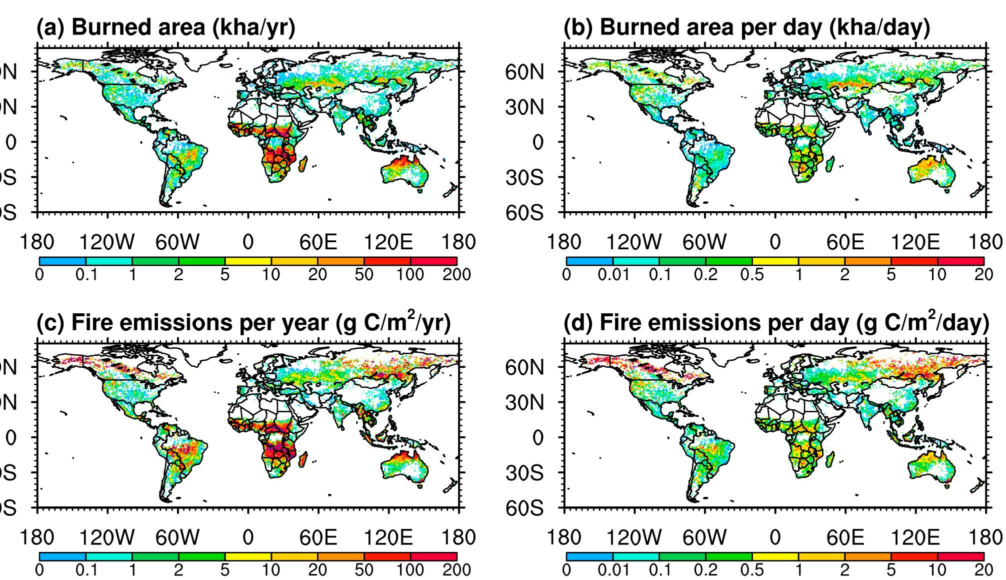

Figure 7. (a) Mean annual burned area (kha/yr), (b) mean burned area per fire day (kha/day), (c) mean annual fire emissions (gC/m^2/yr) and (d) mean annual emissions per day of burning (g C/m^2/day). All panels show mean patterns during 2003–2009. If a grid cell did not have any fires in a given year, this year was excluded from the multiyear mean shown in the panel.

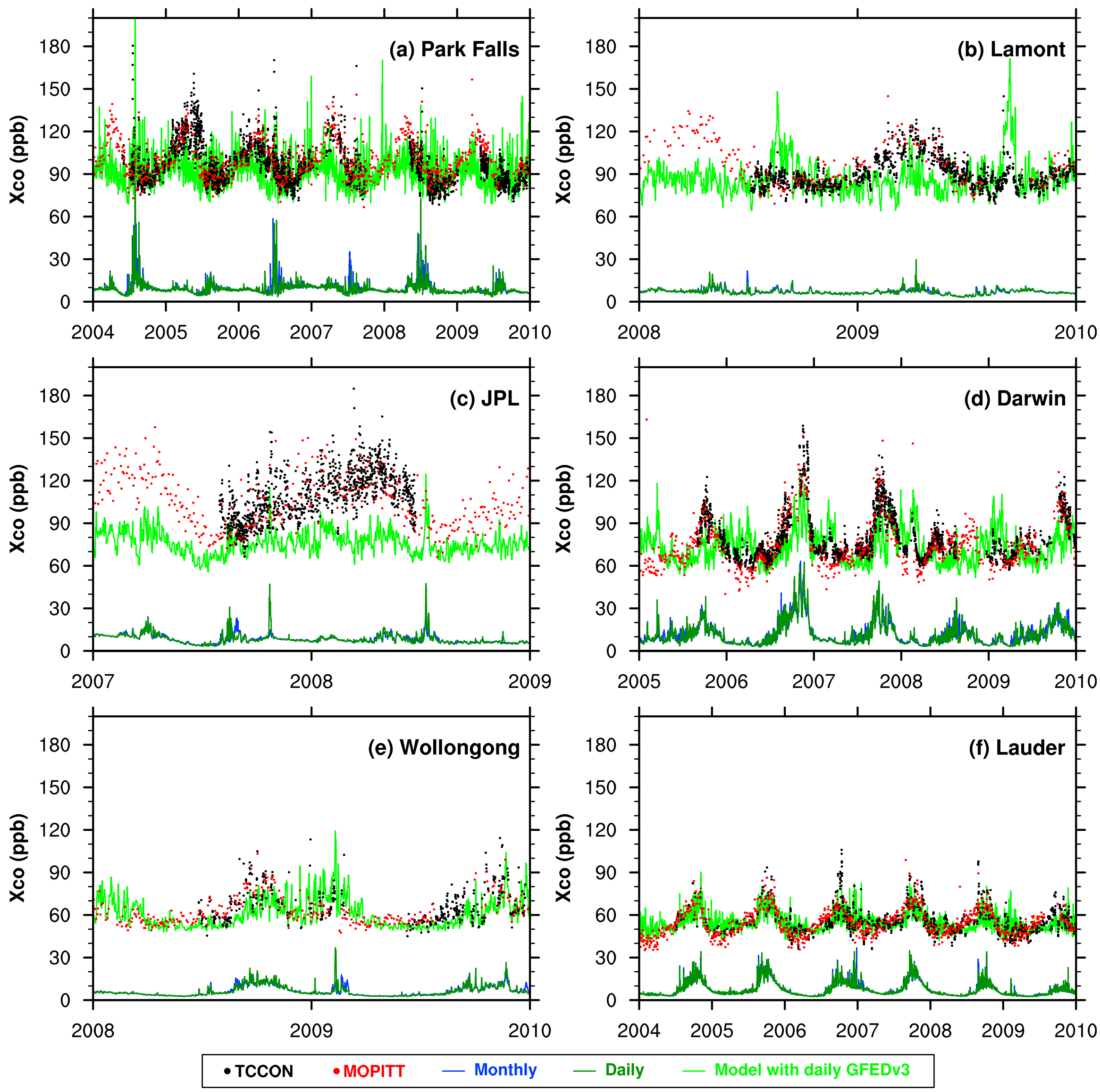

Figure 8. CO column observations and model estimates of the fire contribution to each column observation at: (a) Park Falls, (b) Lamont, (c) JPL, (d) Darwin, (e) Wollongong and (f) Lauder. Black dots show the 3-hourly TCCON observations. Red dots show the MOPITT 4 daily level 3 satellite observations. The model simulations of fire-derived CO are from GEOS-Chem with monthly emissions (blue line) and daily emissions (dark green line). Modeled column total CO including non-fire sources and with daily fire emissions (light green line) are also shown in the figure. Simulations with 3-hourly emissions were very similar to those with daily emissions and thus are not shown. To obtain the model estimates, we first converted the model CO profile to column CO using the appropriate (solar zenith angle-dependent) TCCON averaging kernel for each time point. The MOPITT 4 observations shown here also were transformed to the same scale using the TCCON averaging kernels following the approach described by *Luo et al.* [2007].

of tree cover. *Roberts et al.* [2009], using Spinning Enhanced Visible and Infrared Imager (SEVIRI) data for Africa, documented considerable differences in diurnal cycles for different vegetation types, but with distributions not fully consistent with the mechanisms and observations described above. Future intercomparison efforts to reconcile the differences between these studies may require use of high resolution maps of land cover and multiple fire detection algorithms (e.g., both SEVIRI and GOES_WF_ABBA algorithms) driven by the same set thermal imagery.

[39] The diurnal patterns described above for boreal, temperate and tropical ecosystems appeared to be robust when we performed sensitivity studies examining how the diurnal cycles changed as a function of the quality (and number) of active fire detections included in the analysis (auxiliary material Figure S8). Including GOES WF_ABBA quality classes 0–5 increased the number of active fire observations (and also the number of false detections) and led to diurnal cycles that were broadly similar to the higher quality observations used to develop our diurnal emissions

Table 4. Correlation Coefficients Between TCCON CO Column Observations and GEOS-Chem Simulations With Monthly, Daily and 3-Hourly Fire Emissions (Mean Annual Cycle Not Removed)

		Full Time Series			Peak Fire Season (3 Months)		
TCCON Station	Latitude and Longitude	Monthly	Daily	3-Hourly	Monthly	Daily	3-Hourly
Park Falls, WI	45.945°N 90.273°W	0.26	0.29	0.29	0.13	0.25	0.24
Lamont, OK	36.604°N 97.486°W	0.13	0.14	0.13	0.42	0.47	0.44
JPL, CA	34.200°N 118.180°W	0.27	0.29	0.33	0.54	0.56	0.56
Darwin, AU	12.424°S 130.892°E	0.48	0.53	0.53	0.71	0.80	0.82
Wollongong, AU	34.406°S 150.879°E	0.59	0.60	0.60	0.53	0.56	0.56
Lauder, NZ	45.038°S 169.684°E	0.67	0.67	0.67	0.54	0.56	0.56

climatology. Separate analysis of early, mid and late fire season periods indicated that differences in the diurnal cycles among different vegetation classes were mostly similar during these different periods, although agricultural fires in Central America appeared to shift from peaking later to earlier in the diurnal cycle with progression of the fire season (auxiliary material Figure S9).

3.4. Impacts of Temporal Resolution of Emissions on Atmospheric CO Simulations

[40] At TCCON stations, model simulations indicated that fires contributed to some of the observed variability in CO on synoptic to interannual timescales (Figure 8). At Darwin, for example, fire-derived CO was a dominant contributor to the annual cycle, with mixing ratios peaking during the moderate 2006 El Niño. At Park Falls, in contrast, fire contributions were smaller and occurred primarily during midsummer. Increasing the temporal resolution of fire emissions modestly improved the agreement between the model and the observations at Darwin and Park Falls, particularly when we replaced monthly with daily emissions and analyzed contributions to variability during the peak fire season (Table 4). At Darwin, using daily emissions instead of monthly emissions increased the correlation between the model and the observations from 0.48 to 0.53. During the fire season, the improvements were larger, with the correlation increasing from 0.71 to 0.80 (Figure 9). At other TCCON stations, use of daily emissions instead of monthly emissions had relatively small or virtually no impact on model performance. Further, use of 3-hourly emissions did not significantly improve model performance beyond that obtained from the daily emissions time series at all of these sites.

[41] We conducted a similar analysis using daily level-3 MOPITT4 observations over a set of broad geographic regions. Small improvements in model performance occurred using daily instead of monthly emissions in many regions, including boreal North America, temperate North America, southern hemisphere South America, boreal Asia, Southeast Asia, equatorial Asia, and Australia (Table 5). Higher temporal frequency emissions had almost no effect on model performance in several other regions, including Central America, northern hemisphere South America, and the Middle East. As with the TCCON sites, improvements gained from the use of higher frequency emissions were larger on sub-seasonal timescales (and during peak fire season). The largest improvements in model performance derived from using daily fire emissions estimates occurred over source regions or in nearby outflow regions (Figure 10). Daily emissions increased the correlation between model

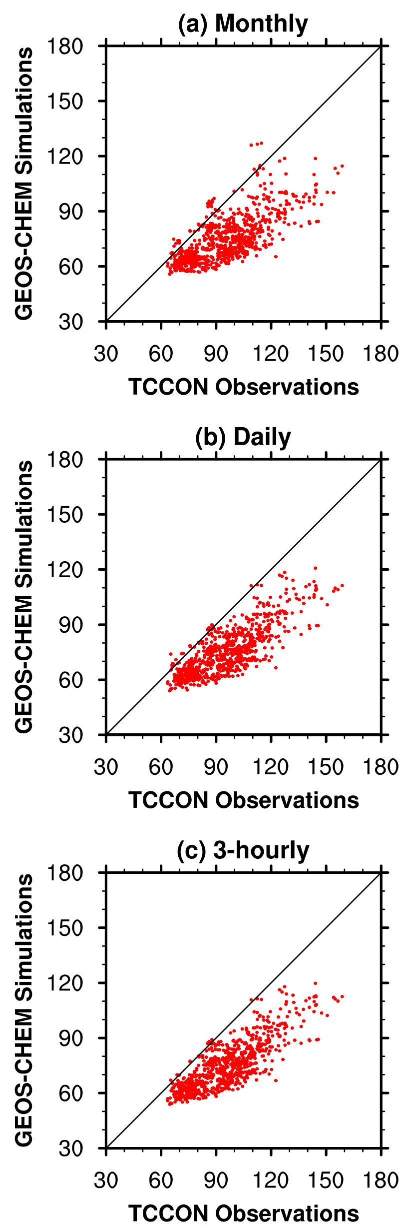

Figure 9. Model versus observed column CO for the Darwin, Australia TCCON site sampled during 3 month intervals during peak fire season each year. (a) Monthly fire emissions model estimates, (b) daily fire emissions model estimates, and (c) 3-hourly fire emissions model estimates. Units are column dry air mole fractions of CO × 10^9 (ppb).

Table 5. Correlations Between MOPITT Column CO and GEOS-Chem Model Simulations With Monthly, Daily, and 3-Hourly Fire Emissions

	Full Time Series[a]			Peak Fire Season (3 Months)		
Region	Monthly	Daily	3-Hourly	Monthly	Daily	3-Hourly
BONA	0.44	0.50	0.50	0.32	0.41	0.42
TENA	0.45	0.47	0.47	0.19	0.23	0.23
CEAM	0.02	0.02	0.02	0.38	0.40	0.40
NHSA	0.18	0.18	0.18	0.26	0.25	0.25
SHSA	0.50	0.52	0.52	0.58	0.61	0.61
EURO	0.68	0.68	0.68	0.36	0.40	0.40
MIDE	0.32	0.32	0.32	−0.07	−0.06	−0.06
NHAF	0.29	0.30	0.30	0.32	0.33	0.33
SHAF	0.62	0.64	0.64	0.60	0.63	0.63
BOAS	0.56	0.59	0.59	0.60	0.65	0.65
CEAS	0.50	0.51	0.51	0.27	0.29	0.29
SEAS	0.44	0.46	0.45	0.43	0.46	0.46
EQAS	0.46	0.48	0.48	0.65	0.70	0.70
AUST	0.53	0.55	0.55	0.54	0.59	0.59

[a]Correlations from 1° × 1° grid cells that had more than 50 valid daily MOPITT 4 observations during 2004–2009 were averaged in each region between 70°N and 50°S.

and MOPITT4 observations considerably in boreal North America and Asia, southern Africa, India, Myanmar, and northern Australia. As expected, in areas far remote from source regions like the mid-Pacific, the impacts of using higher frequency emissions were minimal. This was probably a consequence of substantial atmospheric mixing that attenuated high frequency variability originating from continental source regions.

4. Discussion

[42] High temporal resolution estimates of fire emissions, like the time series we developed here, may allow for more effective attribution of the sources of trace gases and aerosols. This is possible because in many regions fires are often sporadic, creating unique spatial and temporal imprints on atmospheric constituents that, in turn, provide a means for quantifying levels of fire emissions and isolating these contributions from other sources [e.g., *Wang et al.*, 2006]. High temporal resolution emissions estimates also are important for carbon data assimilation systems that often integrate CO_2 observations with other meteorological variables on hourly time scales [*Peters et al.*, 2007; *Zupanski et al.*, 2007]. In addition, daily emissions estimates are needed for air quality studies in regions with high fuel loads near population centers, such as efforts to quantify the human health impacts of peat fires during 2010 across Russia.

4.1. Directions for Future Work

[43] Continuous remote sensing observations of fire radiative energy (FRE) provide an alternate means for estimating emissions [*Wooster et al.*, 2005; *Roberts and Wooster*, 2008] that may enable near real-time aerosol and atmospheric chemistry forecasts [*Kaiser et al.*, 2011]. One important direction for future research is to reconcile top-down estimates

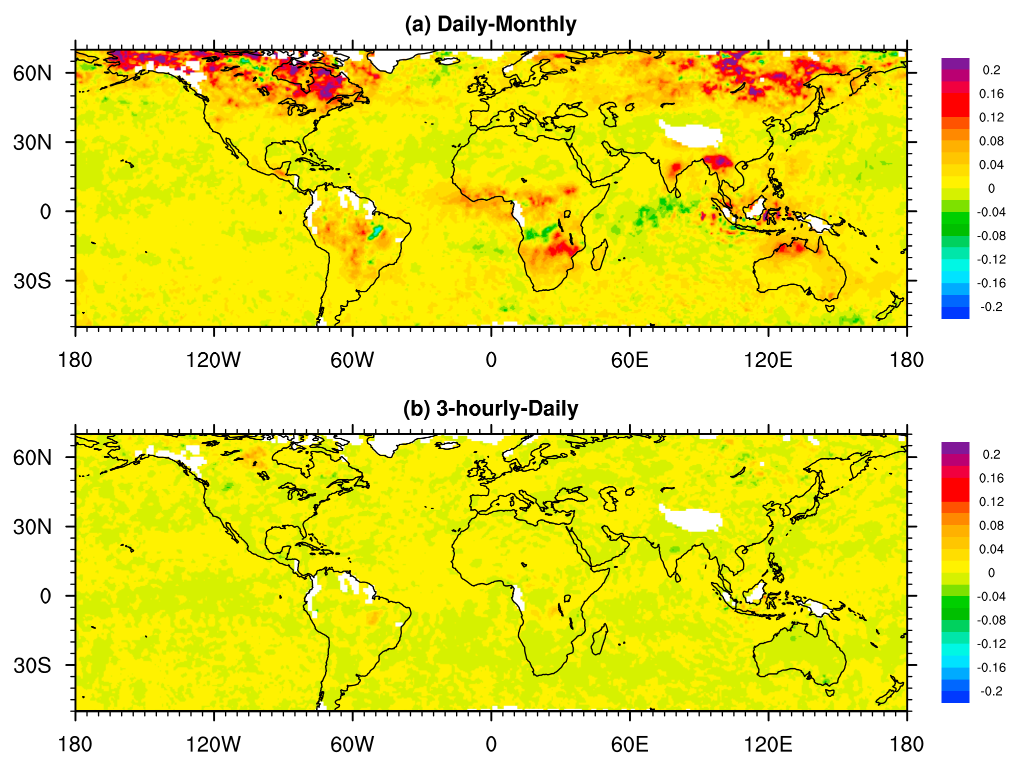

Figure 10. Improvements in model performance obtained from using daily and 3-hourly emissions estimates. The difference in model correlation with MOPITT4 daily level 3 observations is shown for model simulations with (a) daily and monthly emissions and (b) 3-hourly and daily emissions. Prior to estimating the correlation between the model and MOPITT4, a monthly mean annual cycle of CO was removed from both the observations and the model.

of FRE derived from thermal imagery with bottom-up estimates of energy release from forward biogeochemical models [e.g., *Roberts et al.*, 2011]. Figure 7, where we estimated the daily rate of carbon emissions, is a step in this direction. It shows, for example, that boreal fires tend to have significantly higher rates of emissions per day of burning than savanna fires at a 0.5° spatial resolution. Since the energy content of most fuels varies within a relatively narrow range, total burned area and fuel consumption provide a strong constraint on the total energy released by a fire. Active fires from polar orbiting and geostationary sources, in turn, allow for the partitioning of this energy through time, thus allowing for more reasonable forward model estimates of energy release. In this context, the north-south gradients of daily rates of carbon emissions reported here for North American forests appear qualitatively consistent with fire plume heights measured by *Val Martin et al.* [2010]. Both plume heights and daily emissions were at maximum levels in boreal forests in Alaska and Canada, at intermediate levels in temperate forests and shrublands across the U.S., and at minimum levels for tropical forests in southern Mexico, Guatemala, and other countries in northern Central America. Mechanistically, fires that release high levels of carbon each day also would be expected to generate the energy required to inject plumes to higher altitudes within the free troposphere [*Freitas et al.*, 2007]. Deeper and drier atmospheric boundary layers in boreal regions may create conditions that simultaneously enable both higher rates of fuel consumption and higher plumes. A more direct comparison of FRE from forward modeling and satellite-derived approaches will require several additional steps however, including, for example, the availability of emission data with the same spatial resolution as the active fire data (~1 km) and careful consideration of the length and structure of the fire front.

[44] Future improvements in high temporal resolution time series of fire emissions will likely come from several sources, including use of additional satellite observations and consideration of additional fire processes. Burned area estimates derived from surface reflectance changes in many instances can provide daily to-weekly estimates of the perimeter of the fire-affected area [*Tansey et al.*, 2008]. Combining this information with the active fire time series described above has the potential to reduce uncertainties [*Roberts et al.*, 2011]. Importantly, with moderate resolution (e.g., ~500 m) burned area data, it may be possible to interpolate the movement of the fire perimeter over a period of several days- thus filling in gaps created by clouds or intervals between successive satellite overpasses.

[45] In future work on diurnal patterns of fire emissions, it may be possible to systematically relate the amplitude of the diurnal cycle of satellite-derived observations of active fires to key environmental variables such as wind speed, humidity, and fuel moisture [e.g., *Smith and Wooster*, 2005] – drawing upon relationships that are well established in the fire behavior literature. Here we assumed that the diurnal cycles of total carbon, CO_2, and CO emissions were the same as a first approximation. An important future step for reducing uncertainties in emissions will be to allow emission factors for CO and other trace gases and aerosols to vary diurnally. Smoldering combustion, which has greater relative production of reduced gases and aerosols (i.e., lower combustion efficiencies), contributes more to total nighttime emissions than to daytime emissions [e.g., *Ward et al.*, 1992; *Cachier et al.*, 1995; *Hao et al.*, 1996; *Ferguson et al.*, 2003; *Schkolnik et al.*, 2005; *Fuzzi et al.*, 2007] because of higher levels of atmospheric humidity and lower wind speeds during night that tend to suppress flaming stages of combustion [e.g., *Beck and Trevitt*, 1989; *Linn et al.*, 2002; *McRae et al.*, 2005]. More field observations of CO_2, CH_4, and CO over multiple diurnal and seasonal cycles are needed in biomass burning field studies to develop realistic emission factor parameterizations. Deployment of space-based laser spectrometers that measure multiple gases, following for example from NASA mission concepts such as Active Sensing of Carbon Dioxide Emissions over Nights, Days and Seasons (ASCENDS) [*Abshire et al.*, 2010], also have the potential to constrain this variability.

4.2. Sources of Uncertainty

[46] Using a global atmospheric model, here we observed modest improvements in our simulations when we included daily and 3-hourly variability in emissions. There are probably at least four different reasons why the model improvements were not larger. First, even if emissions were known perfectly, other sources of error within the atmospheric modeling framework would be expected to limit simulation performance. For example, we did not use high temporal resolution inventories for several other important sources of CO, including fossil fuel emissions, because these time series are not yet available at a global scale. Uncertainties in several other sources, including biogenic emissions of volatile organic compounds, also are considerable and our understanding of seasonal and interannual controls on these fluxes remains limited. In addition, significant uncertainties exist with respect to several aspects of atmospheric model transport, including for example vertical mixing by convection in the free troposphere, flow in regions with complex terrain, atmospheric boundary layer dynamics, and fire injection processes. The relatively coarse resolution of our atmospheric model (2.5°) also probably damped temporal and spatial variability in simulated atmospheric CO driven by our daily and 3-hourly emissions time series. With future higher spatial resolution simulations (and comparisons with surface CO observations near source regions), we hypothesize that improvements from using the daily and 3-hourly emissions inventories will be more substantial.

[47] Second, at several of the TCCON sites, mostly notably Lamont and Lauder, the contribution from local fire sources was most likely relatively small. Long-range atmospheric transport (e.g., at Lauder, transport of CO from fires in Australia, southern Africa, and South America) is likely to act as a low-pass smoothing filter on emissions as a consequence of diffusive mixing, thus limiting improvements in the model obtained from replacing monthly with daily (or 3-hourly) fire emissions.

[48] Third, important uncertainties remain with respect to quantifying daily variability in emissions. The MODIS active fire time series used here was derived from polar-orbiting Terra and Aqua satellites and as a consequence, gaps in coverage existed in tropical regions. It is likely that this source of uncertainty will be reduced in the future as more geostationary satellite observations of active fires become publicly available for Africa and Asia [*Reid et al.*, 2009], along with more detailed information on fire radiative power

and fire size. Even with the expected future increases in data availability, persistent cloud cover in tropical regions will remain an important challenge with respect to active fire detection and thus to the development of a daily time series of fires driven by either geostationary or polar-orbiting satellite observations.

[49] Fourth, on longer time scales our understanding of several of the key processes regulating emissions remains limited. Over the last decade, improved change detection algorithms and increased availability of high quality moderate resolution surface reflectance data has transformed our understanding of burned area at a global scale and has led to a several-fold reduction in uncertainty, particularly in boreal forest and savanna biomes. Although further improvements in burned area are urgently needed, including improved methods for mapping small (sub-500 m) fires and understory fires in forests, in many regions burned area observations are no longer the primary source of uncertainty in fire emissions estimates. For example, our ability to quantify and develop realistic parameterization of fuel consumption has not progressed as quickly over the last decade, in part from dearth of information on how to scale estimates of tree mortality and combustion completeness across heterogeneous landscapes in savanna, woodland, and tropical forest ecosystems [e.g., *van der Werf et al.*, 2010].

[50] On hourly time-scales, one primary driver of uncertainty is related to diurnal variations in the performance of the active fire detection algorithm. For the 4 μm band, the thermal contrast between fire pixels and neighboring cells is highest at night when the surface is cool and there is no contamination from reflected solar radiation [*Giglio*, 2007]. As a result, the efficacy of the active fire detection algorithm may be higher, particularly for smaller fires. Lower detection efficiencies during the day, when there is less thermal contrast, may lead to an overall reduction in the amplitude of the diurnal cycle. Cooler air and surface temperatures at night, however, also may reduce the likelihood of false detections (which would mostly likely occur during midday) causing a bias in the opposite direction [*Giglio*, 2007; *Schroeder et al.*, 2008]. In this context, evaluating the robustness of the different diurnal cycles measured here for agriculture and grass, shrub, and forest vegetation types (and the relatively small differences in phasing observed between them) will require comparisons with other geostationary active fire products, the use of other land cover maps, coordinated aircraft and field campaigns, and more detailed analysis of diurnal changes in the efficiency of the WF_ABBA algorithm used here.

[51] Other important remaining sources of uncertainty in the diurnal cycle characterizations include the influence of block out zones used to avoid solar contamination near local solar noon. Work is currently underway to evaluate a new generation of spatially gridded global geostationary WF_ABBA active fire products that include information on block outs and other data gaps in the geostationary record. Use of these gridded products in future work may enable a more systematic quantification and reduction of uncertainties related to solar zenith angle effects.

5. Conclusions

[52] Here we developed an approach for representing daily and 3-hourly variability in global fire emissions using a combination of polar-orbiting and geostationary satellite observations of active fires. Outside of the tropics, our time series resolved day-to-day variations in fires. In the tropics, we applied a 3-day center mean smoothing filter to avoid spikiness caused by gaps in coverage by Aqua and Terra satellites. For each month, we constructed a mean diurnal cycle of fire activity in each grid cell based on burned area in different vegetation types and vegetation-specific mean diurnal cycles derived from the GOES WF_ABBA fire product. Our time series was designed for use in global atmospheric studies of trace gases and aerosols. Because of the sporadic nature of fires on synoptic time scales in many regions, high temporal resolution estimates may allow for improved attribution of causes of variations in atmospheric constituents.

[53] Several distinct biome-level differences in fire behavior emerged from our study of daily fires. In boreal biomes, the number of fire days in a given year at a 0.5° spatial resolution rarely exceeded 20 whereas in tropical savannas this often exceeded 100. The duration of fire events (continuous periods of burning) also was shorter in boreal biomes. The abrupt nature of boreal fires, combined with high levels of fuel consumption (g C per m^2 of burned area) caused daily rates of fuel consumption to be over an order of magnitude higher in boreal regions than in savanna regions. Diurnally, observations from GOES WF_ABBA indicated that fires in grasslands, savannas, and crops often occurred earlier in the day than in forests.

[54] Atmospheric model simulations with daily and 3-hourly emissions generally showed improved agreement with ground based and space based remote sensing observations of CO, particularly during the fire season. Directions for future research include reconciling forward model and satellite-derived estimates of fire radiative power and integrating multiple geostationary and polar orbiting fire products to produce higher quality (and higher temporal resolution) emissions time series.

[55] **Acknowledgments.** This research was supported by NASA grants NNX08AF64G and NNX10AT83G and the EU Seventh Research Framework Programme (MACC project, contract 218793). The time series described here is publicly available on the Global Fire Emissions Database server (www.globalfiredata.org). We thank E. Lyons for contributing to the development of the daily fire emissions time series. E. J. Hyer and E. Prins acknowledge support from the NASA Interdisciplinary Studies Program. U.S. funding for TCCON comes from NASA's Terrestrial Ecology Program (NNX08A186G), the Orbiting Carbon Observatory Program (NAS7–03001), the DOE/ARM Program and the Atmospheric CO_2 Observations from Space Program. Some of the research described in this paper was performed at the Jet Propulsion Laboratory, California Institute of Technology, under a contract with the National Aeronautics and Space Administration. The Lauder TCCON measurements were funded by New Zealand Foundation for Research, Science and Technology contracts CO1X0204 and CO1X0406. We thank B. Connor and J. Robinson for their contributions to the Lauder CO time series.

References

Abshire, J. B., et al. (2010), A lidar approach to measure CO_2 concentrations from space for the ASCENDS mission, *Proc. SPIE Int. Soc. Opt. Eng.*, *7832*, 78320D, doi:10.1117/12.868567.

Al-Saadi, J., et al. (2008), Intercomparison of near-real-time biomass burning emissions estimates constrained by satellite fire data, *J. Appl. Remote Sens.*, *2*, 021504, doi: 10.1117/1.2948785.

Arino, O., and J.-M. Rosaz (1999), 1997 and 1998 world ATSR fire atlas using ERS-2 ATSR-2 data, paper presented at Proceedings of the Joint

Fire Science Conference and Workshop, Int. Assoc. of Wildland Fire, Boise, Idaho.
Beall, H. W. (1934), Diurnal and seasonal fluctuation of fire-hazard in pine forests, *For. Chron.*, *10*, 209–225.
Beck, J. A., and A. C. F. Trevitt (1989), Forecasting diurnal-variations in meteorological parameters for predicting fire behavior, *Can. J. For. Res.*, *19*, 791–797, doi:10.1139/x89-120.
Bergamaschi, P., R. Hein, M. Heimann, and P. J. Crutzen (2000), Inverse modeling of the global CO cycle 1. Inversion of CO mixing ratios, *J. Geophys. Res.*, *105*, 1909–1927, doi:10.1029/1999JD900818.
Bey, I., D. J. Jacob, R. M. Yantosca, J. A. Logan, B. D. Field, A. M. Fiore, Q. B. Li, H. G. Y. Liu, L. J. Mickley, and M. G. Schultz (2001), Global modeling of tropospheric chemistry with assimilated meteorology: Model description and evaluation, *J. Geophys. Res.*, *106*(D19), 23,073–23,095, doi:10.1029/2001JD000807.
Boby, L. A., E. A. G. Schuur, M. C. Mack, D. Verbyla, and J. F. Johnstone (2010), Quantifying fire severity, carbon, and nitrogen emissions in Alaska's boreal forest, *Ecol. Appl.*, *20*(6), 1633–1647, doi:10.1890/08-2295.1.
Boersma, K. F., D. J. Jacob, H. J. Eskes, R. W. Pinder, J. Wang, and R. J. van der A (2008), Intercomparison of SCIAMACHY and OMI tropospheric NO_2 columns: Observing the diurnal evolution of chemistry and emissions from space, *J. Geophys. Res.*, *113*, D16S26, doi:10.1029/2007JD008816.
Bousquet, P., et al. (2006), Contribution of anthropogenic and natural sources to atmospheric methane variability, *Nature*, *443*(7110), 439–443, doi:10.1038/nature05132.
Bowman, D., et al. (2009), Fire in the Earth System, *Science*, *324*, 481–484, doi:10.1126/science.1163886.
Cachier, H., et al. (1995), Particulate content of savanna fire emissions, *J. Atmos. Chem.*, *22*, 123–148, doi:10.1007/BF00708185.
Chen, Y., Q. Li, J. T. Randerson, E. A. Lyons, R. A. Kahn, D. L. Nelson, and D. J. Diner (2009), The sensitivity of CO and aerosol transport to the temporal and vertical distribution of North American boreal fire emissions, *Atmos. Chem. Phys.*, *9*(17), 6559–6580, doi:10.5194/acp-9-6559-2009.
Chen, Y., J. T. Randerson, G. R. van der Werf, D. C. Morton, M. Mu, and P. S. Kasibhatla (2010), Nitrogen deposition in tropical forests from savanna and deforestation fires, *Global Change Biol.*, *16*(7), 2024–2038, doi:10.1111/j.1365-2486.2009.02156.x.
Chin, M., T. Diehl, O. Dubovik, T. F. Eck, B. N. Holben, A. Sinyuk, and D. G. Streets (2009), Light absorption by pollution, dust, and biomass burning aerosols: A global model study and evaluation with AERONET measurements, *Ann. Geophys.*, *27*(9), 3439–3464, doi:10.5194/angeo-27-3439-2009.
Deeter, M. N. (2009), MOPITT (Measurements of Pollution in the Troposphere) provisional version 4: Product user's guide, report, MOPITT Algorithm Dev. Team, Atmos. Chem. Div., Natl. Cent. for Atmos. Res., Boulder, Colo.
Deeter, M. N., et al. (2003), Operational carbon monoxide retrieval algorithm and selected results for the MOPITT instrument, *J. Geophys. Res.*, *108*(D14), 4399, doi:10.1029/2002JD003186.
Delfino, R. J., et al. (2009), The relationship of respiratory and cardiovascular hospital admissions to the southern California wildfires of 2003, *Occup. Environ. Med.*, *66*(3), 189–197, doi:10.1136/oem.2008.041376.
Duncan, B. N., R. V. Martin, A. C. Staudt, R. Yevich, and J. A. Logan (2003), Interannual and seasonal variability of biomass burning emissions constrained by satellite observations, *J. Geophys. Res.*, *108*(D2), 4100, doi:10.1029/2002JD002378.
Emmons, L. K., et al. (2004), Validation of Measurements of Pollution in the Troposphere (MOPITT) CO retrievals with aircraft in situ profiles, *J. Geophys. Res.*, *109*(D3), D03309, doi:10.1029/2003JD004101.
Eva, H., and E. F. Lambin (1998), Remote sensing of biomass burning in tropical regions: Sampling issues and multisensor approach, *Remote Sens. Environ.*, *64*(3), 292–315, doi:10.1016/S0034-4257(98)00006-6.
Ferguson, S. A., R. L. Collins, J. Ruthford, and M. Fukuda (2003), Vertical distribution of nighttime smoke following a wildland biomass fire in boreal Alaska, *J. Geophys. Res.*, *108*(D23), 4743, doi:10.1029/2002JD003324.
Fiore, A. M., D. J. Jacob, H. Liu, R. M. Yantosca, T. D. Fairlie, and Q. Li (2003), Variability in surface ozone background over the United States: Implication for air quality policy, *J. Geophys. Res.*, *108*(D24), 4787, doi:10.1029/2003JD003855.
Flanner, M. G., C. S. Zender, J. T. Randerson, and P. J. Rasch (2007), Present-day climate forcing and response from black carbon in snow, *J. Geophys. Res.*, *112*, D11202, doi:10.1029/2006JD008003.
Freitas, S. R., K. M. Longo, R. Chatfield, D. Latham, M. Dias, M. O. Andreae, E. Prins, J. C. Santos, R. Gielow, and J. A. Carvalho (2007), Including the sub-grid scale plume rise of vegetation fires in low resolution atmospheric transport models, *Atmos. Chem. Phys.*, *7*(13), 3385–3398, doi:10.5194/acp-7-3385-2007.
French, N. H. F., et al. (2011), Model comparisons for estimating carbon emissions from North American wildland fire, *J. Geophys. Res.*, *116*, G00K05, doi:10.1029/2010JG001469.
Friedl, M. A., et al. (2002), Global land cover mapping from MODIS: Algorithms and early results, *Remote Sens. Environ.*, *83*(1–2), 287–302, doi:10.1016/S0034-4257(02)00078-0.
Fuzzi, S. et al. (2007), Overview of the inorganic and organic composition of size-segregated aerosol in Rondonia, Brazil, from the biomass-burning period to the onset of the wet season, *J. Geophys. Res.*, *112*, D01201, doi:10.1029/2005JD006741.
Giglio, L. (2007), Characterization of the tropical diurnal fire cycle using VIRS and MODIS observations, *Remote Sens. Environ.*, *108*(4), 407–421, doi:10.1016/j.rse.2006.11.018.
Giglio, L., J. D. Kendall, and R. Mack (2003), A multi-year active fire dataset for the tropics derived from the TRMM VIRS, *Int. J. Remote Sens.*, *24*(22), 4505–4525, doi:10.1080/0143116031000070283.
Giglio, L., I. Csiszar, and C. O. Justice (2006), Global distribution and seasonality of active fires as observed with the Terra and Aqua Moderate Resolution Imaging Spectroradiometer (MODIS) sensors, *J. Geophys. Res.*, *111*, G02016, doi:10.1029/2005JG000142.
Giglio, L., T. Loboda, D. P. Roy, B. Quayle, and C. O. Justice (2009), An active-fire based burned area mapping algorithm for the MODIS sensor, *Remote Sens. Environ.*, *113*(2), 408–420, doi:10.1016/j.rse.2008.10.006.
Giglio, L., J. T. Randerson, G. R. van der Werf, P. S. Kasibhatla, G. J. Collatz, D. C. Morton, and R. S. DeFries (2010), Assessing variability and long-term trends in burned area by merging multiple satellite fire products, *Biogeosciences*, *7*(3), 1171–1186, doi:10.5194/bg-7-1171-2010.
Gillett, N. P., A. J. Weaver, F. W. Zwiers, and M. D. Flannigan (2004), Detecting the effect of climate change on Canadian forest fires, *Geophys. Res. Lett.*, *31*, L18211, doi:10.1029/2004GL020876.
Goetz, S. J., G. J. Fiske, and A. G. Bunn (2006), Using satellite time-series data sets to analyze fire disturbance and forest recovery across Canada, *Remote Sens. Environ.*, *101*(3), 352–365, doi:10.1016/j.rse.2006.01.011.
Guenther, A., T. Karl, P. Harley, C. Wiedinmyer, P. I. Palmer, and C. Geron (2006), Estimates of global terrestrial isoprene emissions using MEGAN (Model of Emissions of Gases and Aerosols from Nature), *Atmos. Chem. Phys.*, *6*, 3181–3210, doi:10.5194/acp-6-3181-2006.
Hao, W. M., D. E. Ward, G. Olbu, and S. P. Baker (1996), Emissions of CO_2, CO, and hydrocarbons from fires in diverse African savanna ecosystems, *J. Geophys. Res.*, *101*, 23,577–23,584, doi:10.1029/95JD02198.
Heald, C. L., D. J. Jacob, P. I. Palmer, M. J. Evans, G. W. Sachse, H. B. Singh, and D. R. Blake (2003), Biomass burning emission inventory with daily resolution: Application to aircraft observations of Asian outflow, *J. Geophys. Res.*, *108*(D21), 8811, doi:10.1029/2002JD003082.
Hicke, J. A., G. P. Asner, E. S. Kasischke, N. H. F. French, J. T. Randerson, G. J. Collatz, B. J. Stocks, C. J. Tucker, S. O. Los, and C. B. Field (2003), Postfire response of North American boreal forest net primary productivity analyzed with satellite observations, *Global Change Biol.*, *9*(8), 1145–1157, doi:10.1046/j.1365-2486.2003.00658.x.
Hyer, E. J., E. S. Kasischke, and D. J. Allen (2007), Effects of source temporal resolution on transport simulations of boreal fire emissions, *J. Geophys. Res.*, *112*, D01302, doi:10.1029/2006JD007234.
Jacob, D. J., B. D. Field, E. Jin, I. Bey, Q. Li, J. A. Logan, and R. M. Yantosca (2002), Atmospheric budget of acetone, *J. Geophys. Res.*, *107*(D11), 4100, doi:10.1029/2001JD000694.
Jacobson, M. Z. (2001), Strong radiative heating due to the mixing state of black carbon in atmospheric aerosols, *Nature*, *409*, 695–697, doi:10.1038/35055518.
Jin, Y., and D. P. Roy (2005), Fire-induced albedo change and its radiative forcing at the surface in northern Australia, *Geophys. Res. Lett.*, *32*, L13401, doi:10.1029/2005GL022822.
Johnson, E. A. (1992), *Fire and Vegetation Dynamics: Studies from the North American Boreal Forest*, 131 pp., Cambridge Univ. Press, Cambridge, U. K., doi:10.1017/CBO9780511623516.
Kaiser, J. W., et al. (2011), Biomass burning emissions estimated with a global fire assimilation system based on observed fire radiative power, *Biogeosci. Discuss.*, *8*, 7339–7398, doi:10.5194/bgd-8-7339-2011.
Kaufman, Y. J., et al. (2005), The effect of smoke, dust, and pollution aerosol on shallow cloud development over the Atlantic Ocean, *Proc. Natl. Acad. Sci. U. S. A.*, *102*, 11,207–11,212, doi:10.1073/pnas.0505191102.
Keppel-Aleks, G., P. O. Wennberg, and T. Schneider (2010), Sources of variations in total column carbon dioxide, *Atmos. Chem. Phys. Discuss.*, *10*, 30,569–30,611, doi:10.5194/acpd-10-30569-2010.
Kopacz, M., et al. (2010), Global estimates of CO sources with high resolution by adjoint inversion of multiple satellite datasets (MOPITT, AIRS, SCIAMACHY, TES), *Atmos. Chem. Phys.*, *10*, 855–876, doi:10.5194/acp-10-855-2010.

Langaas, S. (1992), Temporal and spatial distribution of savanna fires in Senegal and the Gambia, West Africa, 1989–1990, derived from multi-temporal AVHRR night images, *Int. J. Wildland Fire*, *2*(1), 21–36, doi:10.1071/WF9920021.

Langenfelds, R. L., R. J. Francey, B. C. Pak, L. P. Steele, J. Lloyd, C. M. Trudinger, and C. E. Allison (2002), Interannual growth rate variations of atmospheric CO_2 and its $\delta^{13}C$, H_2, CH_4, and CO between 1992 and 1999 linked to biomass burning, *Global Biogeochem. Cycles*, *16*(3), 1048, doi:10.1029/2001GB001466.

Latifovic, R., Z. L. Zhu, J. Cihlar, C. Giri, and I. Olthof (2004), Land cover mapping of north and central America - Global Land Cover 2000, *Remote Sens. Environ.*, *89*(1), 116–127, doi:10.1016/j.rse.2003.11.002.

Linn, R., et al. (2002), Studying wildfire behavior using FIRETEC, *Int. J. Wildland Fire*, *11*, 233–246, doi:10.1071/WF02007.

Luo, M., et al. (2007), Comparison of carbon monoxide measurements by TES and MOPITT: Influence of a priori data and instrument characteristics on nadir atmospheric species retrievals, *J. Geophys. Res.*, *112*, D09303, doi:10.1029/2006JD007663.

Lyons, E. A., Y. F. Jin, and J. T. Randerson (2008), Changes in surface albedo after fire in boreal forest ecosystems of interior Alaska assessed using MODIS satellite observations, *J. Geophys. Res.*, *113*, G02012, doi:10.1029/2007JG000606.

Marlon, J. R., et al. (2008), Climate and human influences on global biomass burning over the past two millennia, *Nat. Geosci.*, *1*, 697–702, doi:10.1038/ngeo313.

McMillan, A. M. S., and M. L. Goulden (2008), Age-dependent variation in the biophysical properties of boreal forests, *Global Biogeochem. Cycles*, *22*, GB2023, doi:10.1029/2007GB003038.

McRae, D. J., J. Z. Jin, S. G. Conard, A. I. Sukhinin, G. A. Ivanova, and T. W. Blake (2005), Infrared characterization of fine-scale variability in behavior of boreal forest fires, *Can. J. For. Res.*, *35*(9), 2194–2206, doi:10.1139/x05-096.

Moritz, M. A., T. J. Moody, M. A. Krawchuk, M. Hughes, and A. Hall (2010), Spatial variation in extreme winds predicts large wildfire locations in chaparral ecosystems, *Geophys. Res. Lett.*, *37*, L04801, doi:10.1029/2009GL041735.

Morton, D. C., R. S. Defries, J. T. Randerson, L. Giglio, W. Schroeder, and G. R. van Der Werf (2008), Agricultural intensification increases deforestation fire activity in Amazonia, *Global Change Biol.*, *14*(10), 2262–2275, doi:10.1111/j.1365-2486.2008.01652.x.

Mouillot, F., and C. B. Field (2005), Fire history and the global carbon budget: A 1 degrees × 1 degrees fire history reconstruction for the 20th century, *Global Change Biol.*, *11*, 398–420, doi:10.1111/j.1365-2486.2005.00920.x.

Nepstad, D. C., et al. (1999), Large-scale impoverishment of Amazonian forests by logging and fire, *Nature*, *398*, 505–508, doi:10.1038/19066.

Nepstad, D., et al. (2004), Amazon drought and its implications for forest flammability and tree growth: A basin-wide analysis, *Global Change Biol.*, *10*, 704–717, doi:10.1111/j.1529-8817.2003.00772.x.

Nevison, C. D., N. M. Mahowald, S. C. Doney, I. D. Lima, G. R. Van der Werf, J. T. Randerson, D. F. Baker, P. Kasibhatla, and G. A. McKinley (2008), Contribution of ocean, fossil fuel, land biosphere, and biomass burning carbon fluxes to seasonal and interannual variability in atmospheric CO_2, *J. Geophys. Res.*, *113*, G01010, doi:10.1029/2007JG000408.

Ott, L. E., J. Bacmeister, S. Pawson, K. Pickering, G. Stenchikov, M. Suarez, H. Huntrieser, M. Loewenstein, J. Lopez, and I. Xueref-Remy (2009), Analysis of convective transport and parameter sensitivity in a single column version of the Goddard Earth Observation System, Version 5, general circulation model, *J. Atmos. Sci.*, *66*, 627–646, doi:10.1175/2008JAS2694.1.

Paton-Walsh, C., N. M. Deutscher, D. W. T. Griffith, B. W. Forgan, S. R. Wilson, N. B. Jones, and D. P. Edwards (2010), Trace gas emissions from savanna fires in northern Australia, *J. Geophys. Res.*, *115*, D16314, doi:10.1029/2009JD013309.

Peters, W., et al. (2007), An atmospheric perspective on North American carbon dioxide exchange: CarbonTracker, *Proc. Natl. Acad. Sci. U. S. A.*, *104*(48), 18,925–18,930, doi:10.1073/pnas.0708986104.

Pierce, R. B., et al. (2009), Impacts of background ozone production on Houston and Dallas, Texas, air quality during the Second Texas Air Quality Study field mission, *J. Geophys. Res.*, *114*, D00F09, doi:10.1029/2008JD011337.

Prentice, I. C., D. I. Kelley, P. N. Foster, P. Friedlingstein, S. P. Harrison, and P. J. Bartlein (2011), Modeling fire and the terrestrial carbon balance, *Global Biogeochem. Cycles*, *25*, GB3005, doi:10.1029/2010GB003906.

Prins, E. M., and W. P. Menzel (1992), Geostationary satellite detection of biomass burning in South-America, *Int. J. Remote Sens.*, *13*(15), 2783–2799, doi:10.1080/01431169208904081.

Prins, E. M., J. M. Feltz, W. P. Menzel, and D. E. Ward (1998), An overview of GOES-8 diurnal fire and smoke results for SCAR-B and 1995 fire season in South America, *J. Geophys. Res.*, *103*(D24), 31,821–31,835, doi:10.1029/98JD01720.

Prins, E. M., J. Schmetz, L. Flynn, D. Hillger, and J. M. Feltz (2001), Overview of current and future diurnal active fire monitoring using a suite of international geostationary satellites, in *Global and Regional Wildfire Monitoring: Current Status and Future Plans*, edited by F. J. Ahern, J. G. Goldammer, and C. O. Justice, pp. 145–170, SPB Acad., Hague, Netherlands.

Ramanathan, V., et al. (2001), Indian Ocean Experiment: An integrated analysis of the climate forcing and effects of the great Indo-Asian haze, *J. Geophys. Res.*, *106*, 28,371–28,398, doi:10.1029/2001JD900133.

Randerson, J. T., G. R. van der Werf, G. J. Collatz, L. Giglio, C. J. Still, P. Kasibhatla, J. B. Miller, J. W. C. White, R. S. DeFries, and E. S. Kasischke (2005), Fire emissions from C_3 and C_4 vegetation and their influence on interannual variability of atmospheric CO_2 and $\delta^{13}CO_2$, *Global Biogeochem. Cycles*, *19*(2), GB2019, doi:10.1029/2004GB002366.

Reid, J. S., R. Koppmann, T. F. Eck, and D. P. Eleuterio (2005), A review of biomass burning emissions part II: Intensive physical properties of biomass burning particles, *Atmos. Chem. Phys.*, *5*, 799–825, doi:10.5194/acp-5-799-2005.

Reid, J. S., et al. (2009), Global monitoring and forecasting of biomass-burning smoke: Description of and lessons from the Fire Locating and Modeling of Burning Emissions (FLAMBE) program, *IEEE J. Sel. Top. Appl. Earth Obs. Remote Sens.*, *2*(3), 144–162, doi:10.1109/JSTARS.2009.2027443.

Rienecker, M. M., et al. (2008), The GEOS-5 Data Assimilation System - Documentation of versions 5.0.1, 5.1.0, and 5.2.0, *NASA/TM-2008–104606*, vol. 27, 118 pp., NASA Goddard Space Flight Cent., Greenbelt, Md.

Roberts, G. J., and M. J. Wooster (2008), Fire detection and fire characterization over Africa using Meteosat SEVIRI, *IEEE Trans. Geosci. Remote Sens.*, *46*(4), 1200–1218, doi:10.1109/TGRS.2008.915751.

Roberts, G., et al. (2009), Annual and diurnal African biomass burning temporal dynamics, *Biogeosciences*, *6*, 849–866, doi:10.5194/bg-6-849-2009.

Roberts, G., et al. (2011), Integration of geostationary FRP and polar-orbiter burned area datasets for an enhanced biomass burning inventory, *Remote Sens. Environ.*, *115*, 2047–2061, doi:10.1016/j.rse.2011.04.006.

Rodgers, C. D., and B. J. Connor (2003), Intercomparison of remote sounding instruments, *J. Geophys. Res.*, *108*(D3), 4116, doi:10.1029/2002JD002299.

Rothermel, R. C., and C. W. Philpot (1973), Predicting changes in chaparral flammability, *J. For.*, *71*, 640–643.

Schkolnik, G., et al. (2005), New analytical method for the determination of levoglucosan, polyhydroxy compounds, and 2-methylerythritol and its application to smoke and rainwater samples, *Environ. Sci. Technol.*, *39*, 2744–2752, doi:10.1021/es048363c.

Schroeder, W., E. Prins, L. Giglio, I. Csiszar, C. Schmidt, J. Morisette, and D. Morton (2008), Validation of GOES and MODIS active fire detection products using ASTER and ETM plus data, *Remote Sens. Environ.*, *112*, 2711–2726, doi:10.1016/j.rse.2008.01.005.

Schulz, M., et al. (2006), Radiative forcing by aerosols as derived from the AeroCom present-day and pre-industrial simulations, *Atmos. Chem. Phys.*, *6*, 5225–5246, doi:10.5194/acp-6-5225-2006.

Show, S. B. (1919), Climate and forest fires in northern California, *J. For.*, *17*, 965–979.

Smith, A. M. S., and M. J. Wooster (2005), Remote classification of head and backfire types from MODIS fire radiative power and smoke plume observations, *Int. J. Wildland Fire*, *14*, 249–254, doi:10.1071/WF05012.

Streets, D. G., Q. Zhang, L. Wang, K. He, J. Hao, Y. Wu, Y. Tang, and G. R. Carmichael (2006), Revisiting China's CO emissions after the Transport and Chemical Evolution over the Pacific (TRACE-P) mission: Synthesis of inventories, atmospheric modeling, and observations, *J. Geophys. Res.*, *111*, D14306, doi:10.1029/2006JD007118.

Swetnam, T. W., and J. L. Betancourt (1998), Mesoscale disturbance and ecological response to decadal climatic variability in the American Southwest, *J. Clim.*, *11*, 3128–3147, doi:10.1175/1520-0442(1998)011<3128:MDAERT>2.0.CO;2.

Tansey, K., J. M. Gregoire, P. Defourny, R. Leigh, J. F. O. Pekel, E. van Bogaert, and E. Bartholome (2008), A new, global, multi-annual (2000–2007) burnt area product at 1 km resolution, *Geophys. Res. Lett.*, *35*, L01401, doi:10.1029/2007GL031567.

Tosca, M. G., J. T. Randerson, C. S. Zender, D. L. Nelson, D. J. Diner, and J. A. Logan (2011), Dynamics of fire plumes and smoke clouds associated with peat and deforestation fires in Indonesia, *J. Geophys. Res.*, *116*, D08207, doi:10.1029/2010JD015148.

Val Martin, M., J. A. Logan, R. A. Kahn, F. Y. Leung, D. L. Nelson, and D. J. Diner (2010), Smoke injection heights from fires in North America: Analysis of 5 years of satellite observations, *Atmos. Chem. Phys.*, *10*(4), 1491–1510, doi:10.5194/acp-10-1491-2010.

van der Werf, G. R., J. T. Randerson, G. J. Collatz, L. Giglio, P. S. Kasibhatla, A. F. Arellano, S. C. Olsen, and E. S. Kasischke (2004), Continental-scale partitioning of fire emissions during the 1997 to 2001 El Niño/La Niña period, *Science*, *303*(5654), 73–76, doi:10.1126/science.1090753.

van der Werf, G. R., D. C. Morton, R. S. DeFries, L. Giglio, J. T. Randerson, G. J. Collatz, and P. S. Kasibhatla (2009), Estimates of fire emissions from an active deforestation region in the southern Amazon based on satellite data and biogeochemical modelling, *Biogeosciences*, *6*(2), 235–249, doi:10.5194/bg-6-235-2009.

van der Werf, G. R., et al. (2010), Global fire emissions and the contribution of deforestation, savanna, agricultural, forest, and peat fires (1997–2008), *Atmos. Chem. Phys. Discuss.*, *10*, 16,153–16,230, doi:10.5194/acpd-10-16153-2010.

Wang, J., S. A. Christopher, U. S. Nair, J. S. Reid, E. M. Prins, J. Szykman, and J. L. Hand (2006), Mesoscale modeling of Central American smoke transport to the United States: 1. "Top-down" assessment of emission strength and diurnal variation impacts, *J. Geophys. Res.*, *111*, D05S17, doi:10.1029/2005JD006416.

Wang, J., S. C. van den Heever, and J. S. Reid (2009), A conceptual model for the link between Central American biomass burning aerosols and severe weather over the south central United States, *Environ. Res. Lett.*, *4*(1), 015003, doi:10.1088/1748-9326/4/1/015003.

Ward, D. E., R. A. Susott, J. B. Kauffman, R. E. Babbitt, D. L. Cummings, B. Dias, B. N. Holben, Y. J. Kaufman, R. A. Rasmussen, and A. W. Setzer (1992), Smoke and fire characteristics for cerrado and deforestation burns in Brazil: Base-B experiment, *J. Geophys. Res.*, *97*, 14,601–14,619, doi:10.1029/92JD01218.

Westerling, A. L., et al. (2006), Warming and earlier spring increase western US forest wildfire activity, *Science*, *313*, 940–943, doi:10.1126/science.1128834.

Wiedinmyer, C., B. Quayle, C. Geron, A. Belote, D. McKenzie, X. Y. Zhang, S. O'Neill, and K. K. Wynne (2006), Estimating emissions from fires in North America for air quality modeling, *Atmos. Environ.*, *40*(19), 3419–3432, doi:10.1016/j.atmosenv.2006.02.010.

Wooster, M. J., G. Roberts, G. L. W. Perry, and Y. J. Kaufman (2005), Retrieval of biomass combustion rates and totals from fire radiative power observations: FRP derivation and calibration relationships between biomass consumption and fire radiative energy release, *J. Geophys. Res.*, *110*, D24311, doi:10.1029/2005JD006318.

Wunch, D., P. O. Wennberg, G. C. Toon, G. Keppel-Aleks, and Y. G. Yavin (2009), Emissions of greenhouse gases from a North American megacity, *Geophys. Res. Lett.*, *36*, L15810, doi:10.1029/2009GL039825.

Wunch, D., et al. (2010), Calibration of the Total Carbon Column Observing Network using aircraft profile data, *Atmos. Meas. Tech.*, *3*, 1351–1362, doi:10.5194/amt-3-1351-2010.

Wunch, D., G. C. Toon, J.-F. L. Blavier, R. A. Washenfelder, J. Notholt, B. J. Connor, D. W. T. Griffith, V. Sherlock, and P. O. Wennberg (2011), The Total Carbon Column Observing Network, *Philos. Trans. R. Soc, A*, *369*, 2087–2112, doi:10.1098/rsta.2010.0240.

Xian, P., J. S. Reid, J. F. Turk, E. J. Hyer, and D. L. Westphal (2009), Impact of modeled versus satellite measured tropical precipitation on regional smoke optical thickness in an aerosol transport model, *Geophys. Res. Lett.*, *36*, L16805, doi:10.1029/2009GL038823.

Xu, W., M. J. Wooster, G. Roberts, and P. Freeborn (2010), New GOES imager algorithms for cloud and active fire detection and fire radiative power assessment across North, South and Central America, *Remote Sens. Environ.*, *114*(9), 1876–1895, doi:10.1016/j.rse.2010.03.012.

Yang, Z., R. A. Washenfelder, G. Keppel-Aleks, N. Y. Krakauer, J. T. Randerson, P. P. Tans, C. Sweeney, and P. O. Wennberg (2007), New constraints on Northern Hemisphere growing season net flux, *Geophys. Res. Lett.*, *34*, L12807, doi:10.1029/2007GL029742.

Yevich, R., and J. A. Logan (2003), An assessment of biofuel use and burning of agricultural waste in the developing world, *Global Biogeochem. Cycles*, *17*(4), 1095, doi:10.1029/2002GB001952.

Yu, H., et al. (2006), A review of measurement-based assessments of the aerosol direct radiative effect and forcing, *Atmos. Chem. Phys.*, *6*, 613–666, doi:10.5194/acp-6-613-2006.

Zhang, X. Y., and S. Kondragunta (2008), Temporal and spatial variability in biomass burned areas across the USA derived from the GOES fire product, *Remote Sens. Environ.*, *112*(6), 2886–2897, doi:10.1016/j.rse.2008.02.006.

Zupanski, D., A. S. Denning, M. Uliasz, M. Zupanski, A. E. Schuh, P. J. Rayner, W. Peters, and K. D. Corbin (2007), Carbon flux bias estimation employing maximum likelihood ensemble filter (MLEF), *J. Geophys. Res.*, *112*, D17107, doi:10.1029/2006JD008371.

G. J. Collatz and D. Morton, NASA Goddard Space Flight Center, Biospheric Sciences Research Code 614.4, Greenbelt, MD 20771, USA. (george.j.collatz@nasa.gov; douglas.morton@nasa.gov)

R. S. DeFries, Department of Ecology, Evolution, and Environmental Biology, Columbia University, 10th Fl., Schermerhorn Ext., New York, NY 10027, USA. (rd2402@columbia.edu)

L. Giglio, Department of Geography, University of Maryland, LeFrak Hall, College Park, MD 20742, USA. (giglio@hermes.geog.umd.edu)

D. W. T. Griffith, School of Chemistry, University of Wollongong, Northfields Avenue, Wollongong, NSW 2522, Australia. (griffith@uow.edu.au)

E. J. Hyer, Marine Meteorology Division, Naval Research Laboratory, Monterey, CA 93943, USA. (edward.hyer@nrlmry.navy.mil)

P. Kasibhatla, Nicholas School of the Environment and Earth Sciences, Duke University, Box 90328, Durham, NC 27708, USA. (psk9@duke.edu)

M. Mu and J. T. Randerson, Department of Earth System Science, University of California, Croul Hall, Irvine, CA 92697, USA. (mmu@uci.edu; jranders@uci.edu)

E. M. Prins, Madison Cooperative Institute for Meteorological Satellite Studies, University of Wisconsin-Madison, Madison, WI 53706, USA. (elaine.prins@ssec.wisc.edu)

V. Sherlock, National Institute of Water and Atmospheric Research Ltd., 295-301 Evans Bay Parade, Private Bag 14-901, Kilbirnie, Wellington 6021, New Zealand. (v.sherlock@niwa.co.nz)

G. C. Toon, Jet Propulsion Laboratory, California Institute of Technology, 4800 Oak Grove Dr., Pasadena, CA 91109, USA. (geoffrey.c.toon@jpl.nasa.gov)

G. R. van der Werf, Faculty of Earth and Life Sciences, VU University Amsterdam, De Boelelaan 1085, NL-1081 HV Amsterdam, Netherlands. (guido.van.der.werf@falw.vu.nl)

P. O. Wennberg and D. Wunch, Division of Engineering and Applied Science, California Institute of Technology, 1200 E. California Blvd., Pasadena, CA 91125, USA. (wennberg@gps.caltech.edu; dwunch@caltech.edu)